Journal of Hazardous Materials 424 (2022) 127427

Contents lists available at ScienceDirect

Journal of Hazardous Materials

journal homepage: www.elsevier.com/locate/jhazmat

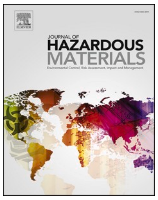

Review

Recent progress in single-atom alloys: Synthesis, properties, and applications in environmental catalysis

Zhiling Xu [a,b], Zhimin Ao [a,*], Mei Yang [b], Shaobin Wang [c]

[a] Guangzhou Key Laboratory Environmental Catalysis and Pollution Control, Guangdong Key Laboratory of Environmental Catalysis and Health Risk Control, School of Environmental Science and Engineering, Institute of Environmental Health and Pollution Control, Guangdong University of Technology, Guangzhou 510006, China
[b] SINOPEC Maoming Petrochemical Company, Maoming 525011, China
[c] School of Chemical Engineering and Advanced Materials, University of Adelaide, Adelaide, SA 5005, Australia

ARTICLE INFO

Editor: Dr. Danmeng Shuai

Keywords:
Single-atom alloys
Environmental catalysis
Catalyst design
Gas pollutants

ABSTRACT

Heterogeneous catalysts have made outstanding advancements in pollutants elimination as well as energy and materials production over the past decades. Single-atom alloys (SAAs) are novel environmental catalysts prepared by dispersing single metal atoms on other metals. Integrating the advantages of single atom and alloys, SAAs can maximize atom utilization, reduce the use of noble metals and enhance catalytic performances. The synergistic, electronic and geometric effects of SAAs are effective to modulate the activation energy and adsorption strength, consequently breaking linear scaling relationship as well as offering an excellent catalytic activity and selectivity. Moreover, SAAs possess clear atomic structure, active sites and reaction mechanisms, providing an opportunity to tailor catalytic properties and develop effective environmental catalysts. In this review, we provide the recent progress on synthetic strategies, catalytic properties and catalyst design of SAAs. Furthermore, the applications of SAAs in environmental catalysis are introduced towards catalytic conversion and elimination of different air pollutants in many important reactions including (electrochemical) oxidation of volatile organic compounds (VOCs), dehydrogenation of VOCs, CO_2 conversion, NO_x reduction, CO oxidation, SO_3 decomposition, etc. Finally, challenges and opportunities of SAAs in a broad environmental field are proposed.

1. Introduction

During the processes of industrialization and urbanization, large consumption of finite reserved fossil fuels and increasingly serious environmental issues cause a big challenge for human health, environmental protection and energy demand (Ibrahim et al., 2016; Silas et al., 2020). More and more efforts have been focused on removal of environmental pollutants, development of clean energy and production of valuable chemicals through green, highly efficient and low-cost technologies (Jones, 2018; Wen et al., 2014). Among various approaches, catalysis plays a crucial role in reducing production costs and enhancing reaction efficiency, which will dramatically improve the development of human society (Parvulescu and Fechete, 2018). Typically, homogeneous catalysts have well-defined structures with an excellent catalytic performance but are limited by poor stability and recyclability (Bender et al., 2018; Sordakis et al., 2018). The utilization of heterogeneous catalysts is then considered as an effective way for environmental applications owing to the high potential in separation, reusability and stability (Shimizu and Satsuma, 2011). Although a great progress has been made in heterogeneous catalysts, it remains a considerable challenge to develop catalysts with high atom utilization efficiency, high catalytic selectivity and well-defined active sites (Hou et al., 2020; Liu and Corma, 2018). Recently, single-atom catalysts (SACs), with atomically dispersed metal atoms, facilitate the maximized atom utilization efficiency to reduce catalyst cost and inherit the advantages of heterogeneous and homogeneous catalysts for many applications (Li et al., 2019; Wang et al., 2018). SACs possess well-defined active sites and unique electronic structures, consequently exhibiting excellent catalytic performances with ultrahigh activity and selectivity (Chen et al., 2018; Gawande et al., 2020).

In particular, an alternative approach have been developed by dispersing isolated metal atoms on the surface of other host metal substrates for producing single-atom alloys (SAAs) (Fig. 1) (Hannagan et al., 2020a). Integrating the advantages of single atom and metal alloys,

---

* Corresponding author.
E-mail address: zhimin.ao@gdut.edu.cn (Z. Ao).

https://doi.org/10.1016/j.jhazmat.2021.127427
Received 6 August 2021; Received in revised form 19 September 2021; Accepted 1 October 2021
Available online 8 October 2021
0304-3894/© 2021 Elsevier B.V. All rights reserved.

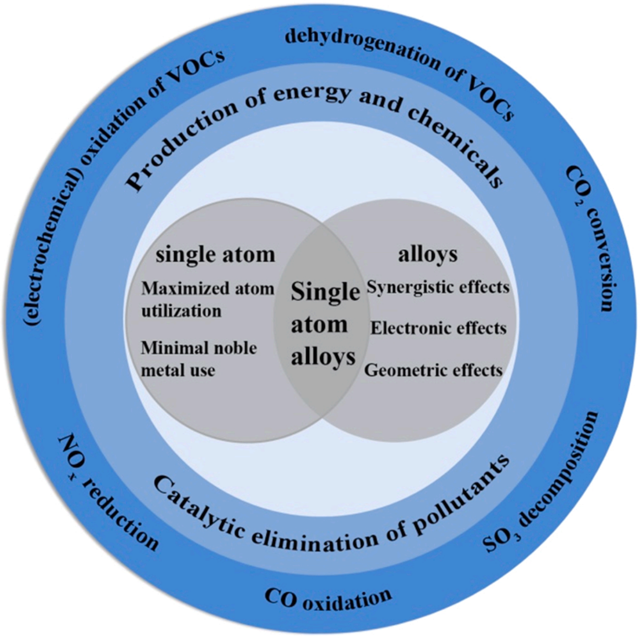

Fig. 1. Single atom alloys (SAAs) inherit the advantages of single atom and alloys, which can maximize atom utilization to reduce the use of noble metal and boost catalytic properties by synergistic, electronic and geometric effects. SAAs hold the potential in applications of environmental catalysis including production of clean energy and valuable chemicals as well as catalytic elimination of pollutants. SAAs exhibit excellent performance towards diverse reactions such as (electrochemical) oxidation of volatile organic compounds (VOCs), dehydrogenation of VOCs, CO_2 conversion, NO_x reduction, CO oxidation, SO_3 decomposition, etc.

SAAs have rapidly become a new research frontier in the field of materials science and catalysis from both theoretical and experimental studies (Giannakakis et al., 2019; Han et al., 2021). SAAs were firstly demonstrated for facile hydrogen dissociation, spillover, and selective hydrogenation reaction on $Pd_1/Cu(111)$ SAAs by Sykes's group (Kyriakou et al., 2012). So far, SAAs have been widely explored for a great variety of reactions such as hydrogenation (Pei et al., 2015), dehydrogenation (Marcinkowski et al., 2018), oxidation (Zhang et al., 2014), hydrogenolysis (Yang et al., 2018), photocatalysis (Pan et al., 2020), and electrocatalysis (Zhang et al., 2019). Generally, SAAs exhibit the unique catalytic performances due to maximizing atom efficiency stemmed from single atom and modulating catalytic properties originated from alloying effects (Mao et al., 2020). The very small quantities of individually dispersed active metal atoms have a substantial effect on the catalytic properties of the host metal substrates through synergistic, electronic and geometric effects (Pei et al., 2017). SAAs are aimed to integrate the distinct superiority of both metals to simultaneously participate in the catalytic process or individually serve for different reaction (Liu et al., 2017). Besides, SAAs possess remarkable electronic and geometric characteristics distinct from single-element metal to provide specific active sites and tune the reaction pathway, consequently boosting high activity and selectivity (Li et al., 2017). Moreover, SAAs can facilitate the activation of reactants by lowering energy barrier towards a high activity and then weaken the adsorption of intermediates for a high selectivity (Darby et al., 2018b). As a consequence, SAAs are capable of breaking the Brønsted−Evans−Polanyi (BEP) relationships between activation barrier and reaction energy to simultaneously offer a high activity and selectivity, which is the general restriction of many catalysts ((Sun et al., 2018; Zhang et al., 2019).

It is of great significance for the rational design of effective SAA catalysts by fundamentally understanding surface structure, active sites and reaction mechanisms. Generally, atomic level understanding of SAAs structure is important to establish definitive structure-property relationships, thereby facilitating systematically tailoring catalytic properties and developing various applications (Zhang et al., 2021). A variety of advanced atomic-resolution characterization techniques have been applied for the study of SAAs structures such as scanning tunneling microscopy (STM), aberration-corrected high-angle annular dark field imaging scanning transmission electron microscopy (HAADF-STEM), and X-ray absorption fine structure (XAFS) spectroscopy (Liu et al., 2020). In addition, the combination of in-situ characterization methods and various surface science experiments can well elucidate the surface structure and even study structural change under reaction conditions, which finely tune the selectivity and activity to guide the catalyst design (Lucci et al., 2015b; Yang et al., 2021). Moreover, the clear and uniform structure of SAAs is useful for the identification of the active sites through *in-situ* characterizations, density functional theory (DFT) calculations, and experimental investigations, which provides an opportunity to improve the existing catalysts and design new catalysts with excellent performance (Lucci et al., 2015a; Yang and Yang, 2018). Furthermore, the well-defined active sites of SAAs facilitate establishing reaction mechanism by the integrated studies of surface science, theory, and catalysis, which is of particular interest in the exploration of highly efficient SAA catalysts and the identification of the key steps involved in reactions (Cao et al., 2020; Liu et al., 2019).

The maximized atomic efficiency and unique catalytic properties of SAAs are particularly appealing for environmental catalysis with low cost and high efficiency (Fig. 2). Many recent researches of SAAs were well summarized in several reviews which demonstrated that SAAs possess excellent catalytic performance in various fields (Han et al., 2019; Hannagan et al., 2020a; Mao et al., 2020). SAAs can likewise be applied in the field of environmental practice, potentially opening an opportunity to incorporate catalysis into solving various environmental problems. However, to the best of our knowledge, no review has yet comprehensively overviewed SAAs for environmental applications in the catalytic elimination of environmental pollutants, development of clean energy and production of high value-added chemicals. Besides, the rational design of SAA catalysts has not yet summarized from understanding surface structure, active sites and reaction mechanisms. In this review, we present the recent progress of SAAs in the synthetic procedures, catalytic properties, catalyst design and environmental catalysis. First, the preparation methods of SAAs are systematically summarized and their merits and demerits are thoroughly compared. Next, catalytic properties and catalyst design of SAAs are well presented. SAAs exhibited unique catalytic performances and can break linear scaling relationships. Catalyst design of SAAs was summarized through fundamentally understanding surface structure, active sites and reaction mechanisms, which were studied by theoretical calculations, advanced characterization techniques and catalytic evaluations. Furthermore, applications in environmental catalysis of SAAs are introduced in the degradation of pollutants, exploration of clean energy and production of valuable chemicals based on different sorts of air pollutants including volatile organic compounds (VOCs) and toxic inorganic gases. The recent developments of SAA catalysts in environmental applications are summarized towards important reactions such as (electrochemical) oxidation of VOCs, dehydrogenation of VOCs, CO_2 conversion, NO_x reduction, CO oxidation, and SO_3 decomposition. Finally, the challenges and prospects of SAAs on the future research in the environmental field are discussed.

2. Synthesis strategies of SAAs

A prerequisite for studying catalytic performances of SAAs is to disperse single metal atoms on another metal, forming stable SAA surface for modelling study or SAA nanoparticle (NPs) for practical applications. Controlled and large-scale synthesis of stable SAAs remains a considerable challenge due to the aggregation tendency of single atoms to large particles (Yang et al., 2013). To date, several methods have been

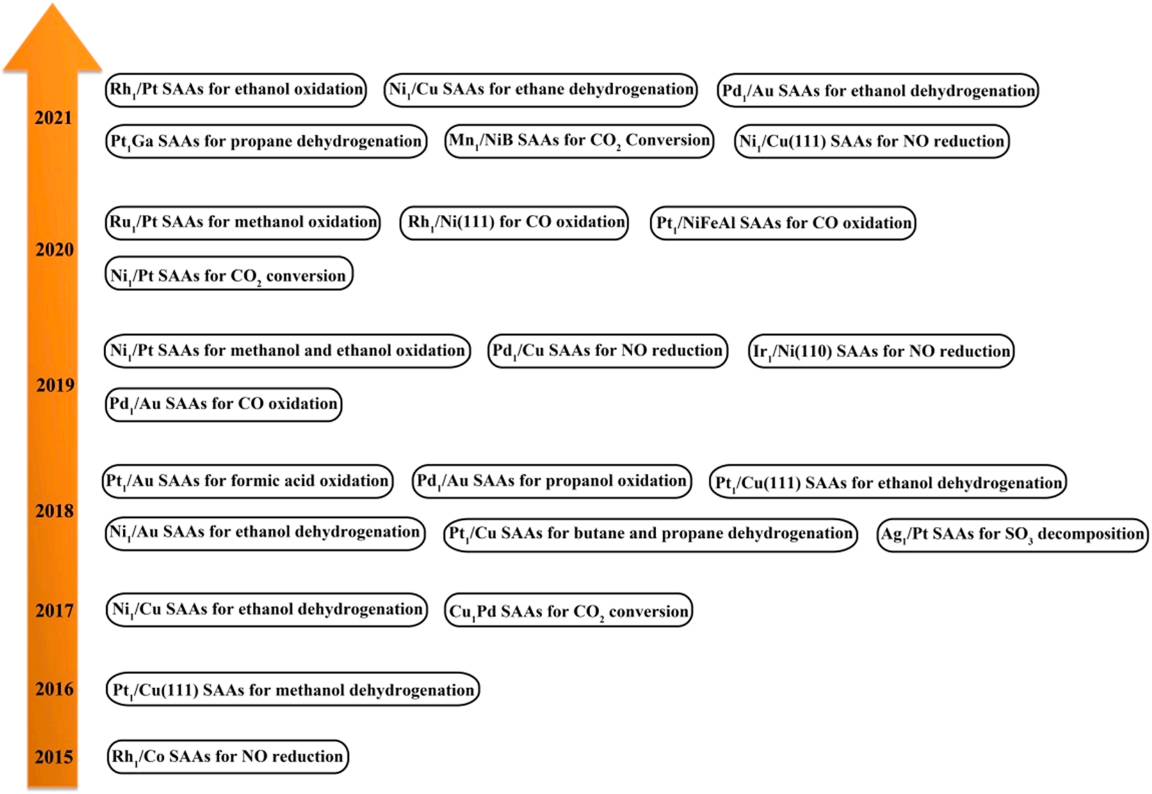

Fig. 2. Timeline of the major breakthroughs regarding SAAs for applications in environmental catalysis from 2015 to 2021.

developed to synthesize SAAs such as physical vapor deposition (PVD), atomic layer deposition (ALD), and wet-chemistry routes. Wet-chemistry routes include incipient wetness impregnation, galvanic replacement and successive reduction method (Fig. 3).

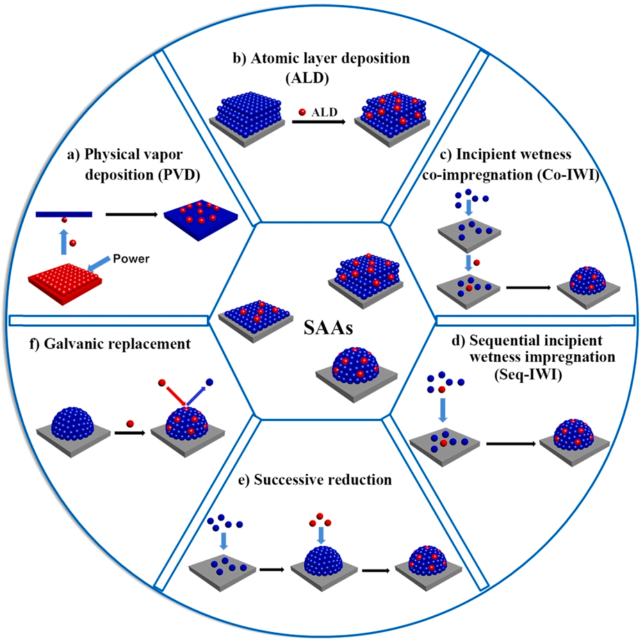

Fig. 3. Schematic illustrations of various synthetic methods of SAAs. (a) Physical vapor deposition (PVD). (b) Atomic layer deposition (ALD). (c) Incipient wetness co-impregnation (Co-IWI). (d) Sequential incipient wetness impregnation (Seq-IWI). (e) Galvanic replacement. (f) Successive reduction.

2.1. *PVD route*

PVD route is linked to transfer materials at the atomic level via electron beams evaporators under vacuum, achieving vapor deposition of isolated metal atoms onto the second metal (Fig. 3a) (Baptista et al., 2018). For example, Kyriakou et al. (2012) utilized PVD method to alloy single palladium (Pd) atoms into Cu(111) surface (Fig. 4a). STM was used to characterize the local atomic arrangement of individual atom on SAAs surface. The STM image of $Pd_1/Cu(111)$ SAAs showed that Pd atoms were deposited preferentially above the step edges (Fig. 4b). Besides, platinum (Pt) single atoms were also embedded into Cu(111) surface by the PVD method with random distribution across both terraces and regions near the step edges (Fig. 4c) (Marcinkowski et al., 2018). By engineering the alloying temperature, Pt atoms were mainly deposited on the surface layer in a monodispersive state. And Pd_1/Au (111) SAAs were formed by the vapor deposition of Pd atoms on Au (111), in which a part of Au lattice was replaced with Pd single atom at the low Pd coverage (Fig. 4d) (Lucci et al., 2016).

2.2. *ALD route*

ALD route is a variation of chemical vapor deposition method through sequential and self-limiting chemical reactions between metal precursor and the surface (Fig. 3b) (George, 2010). ALD method has proven to be successful in the synthesis of the supported bimetallic NPs with the control in size, morphology and composition (Lu et al., 2014). Wang et al. (2019) explored the synthesis of Pd_1/Ni SAAs with isolated Pd atoms dispersed within the outermost layer of Ni NPs using the ALD method (Fig. 4e). The aberration-corrected HAADF-STEM can be used to directly observe single atom on metal hosts by image contrast due to their different atomic numbers. It was suggested that Pd atoms were highly diluted on the partially oxidized Ni NPs from HAADF-STEM image along with intensity profile (Fig. 4f, g).

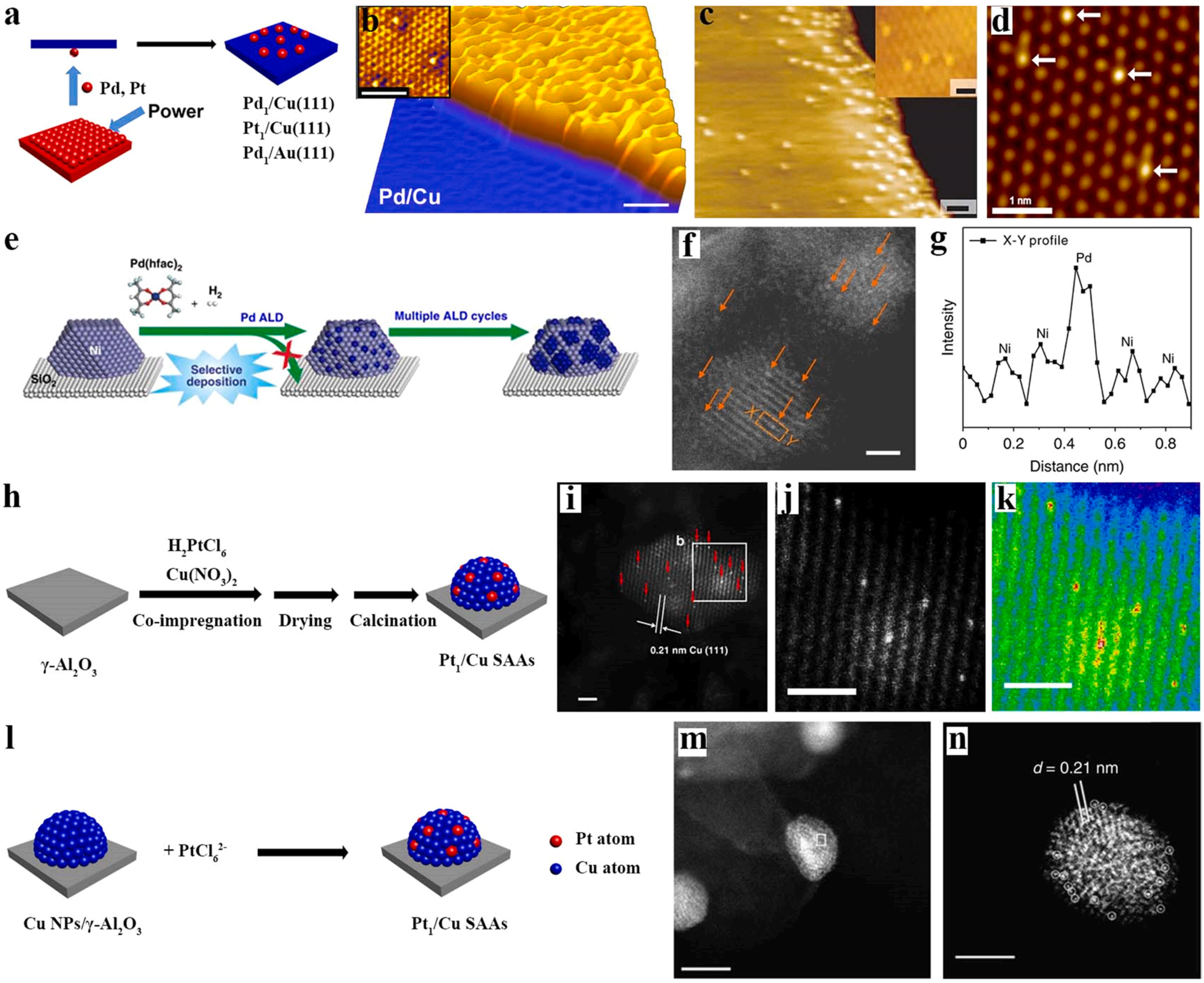

Fig. 4. (a) Schematic description of synthesis of SAAs by PVD method. (b) STM images of $Pd_1/Cu(111)$ SAAs (scale bar, 5 nm). Inset is the atomic resolution image of the $Pd_1/Cu(111)$ SAAs on the upper terrace (scale bar, 2 nm). (c) Wide-scale STM image of $Pt_1/Cu(111)$ SAAs (scale bar, 1 nm). Inset is the atomic resolution image of the alloy surface (scale bar, 0.5 nm). (d) STM image of $Pd_1/Au(111)$ SAAs. (e) Schematic description of synthesis of Pd_1/Ni SAAs supported on SiO_2 by ALD method. (f) The HAADF-STEM image of Pd_1/Ni SAAs prepared by five ALD cycles (scale bar, 2 nm). Pd single atoms were highlighted by brown arrows. (g) Intensity profile along the line X–Y in f. (h) A schematic description of Pt_1/Cu SAA NPs supported on γ-Al_2O_3 formed by the Co-IWI method. (i) HAADF-STEM images of $Pt_{0.1}Cu_{10}/Al_2O_3$. Pt single atoms were marked by red arrows. (j, k) The enlarged image and the colored intensity map from the selected region in a. (l) Schematic illustration of Pt_1/Cu SAA NPs prepared by the replacement reaction method. (m, n) HAADF-STEM images of $Pt_{0.1}Cu_{14}/Al_2O_3$ (scale bars: b, 5 nm; c, 2 nm).
(b) Reproduced with permission Kyriakou et al. (2012). Copyright 2012, American Association for the Advancement of Science. (c) Reproduced with permission Marcinkowski et al. (2018). Copyright 2018, Springer Nature. (d) Reproduced with permission Lucci et al. (2016). Copyright 2016, American Chemical Society. (e-g) Reproduced with permission Wang et al. (2019). Copyright 2019, Springer Nature. (h-k) Reproduced with permission Sun et al. (2018). Copyright 2018, Springer Nature. (l-n) Reproduced with permission Lucci et al. (2015a). Copyright 2015, Springer Nature.

2.3. Wet-chemistry routes

The wet chemistry methods do not require special equipment and are easily operated in experimental conditions. Therefore, wet-chemistry methods are commonly used for the synthesis of SAAs, including incipient wetness impregnation, galvanic replacement and successive reduction method.

2.3.1. Incipient wetness impregnation method

Typically, the incipient wetness impregnation method begins with the first impregnation of two different metal precursors, followed by a drying and calcination process, and concluded with a reduction process. Depending on the impregnation sequence of two metal precursor solutions, incipient wetness impregnation method is divided into incipient wetness co-impregnation (Co-IWI) and sequential incipient wetness impregnation (Seq-IWI). Co-IWI is related to introducing the mixed solution of two metal precursors (Fig. 3c) (Pei et al., 2017). Seq-IWI is concerned with the successive impregnation of two different metal solutions (Fig. 3d) (Cao et al., 2015). For example, Sun et al. (2018) synthesized γ-Al_2O_3-supported Pt_1/Cu SAAs by co-impregnating mixed solutions of H_2PtCl_6 and $Cu(NO_3)_2$ into γ-Al_2O_3 followed by drying and calcination (Fig. 4h). The HAADF-STEM image clearly revealed that the brighter Pt atoms were individually dispersed on Cu NPs (Fig. 4i–k). The lattice spacing of Pt_1/Cu SAAs was 0.21 nm, which agreed with the lattice spacing of Cu(111), indicating that Pt atoms were highly diluted in Cu NPs. Aich et al. (2015) prepared Pd_1/Ag SAA NPs through Co-IWI or Seq-IWI method and evaluated the catalytic activity for acrolein hydrogenation. In the Seq-IWI process, $Pd(NO_3)_2$ and $AgNO_3$ solutions were separately dissolved in water and consecutively impregnated into SiO_2 followed by the reduction treatments.

2.3.2. Galvanic replacement method

Galvanic replacement method is involved in an electrochemical reaction between one metal (template) and the other metal ions possessing a higher reduction potential, which are reduced and deposited on the template (Fig. 3e) (Xia et al., 2013). For instance, Boucher et al. (2013b) employed the galvanic replacement method for the synthesis of Pd_1/Cu SAA NPs by replacing Cu with a trace amount of Pd in Cu/Al_2O_3 NPs. Lucci et al. (2015a) prepared Pt_1/Cu SAAs supported on γ-Al_2O_3 by the galvanic replacement method for selective hydrogenation of butadiene (Fig. 4l). The differences in Z-contrast confirmed the existence of isolated Pt atoms distributed on Cu NPs from HAADF-STEM, clearly demonstrating the formation of Pt_1/Cu SAA NPs (Fig. 4m). In addition, the highly diluted dispersion of Pt atoms was revealed by the consistent lattice spacing of Pt_1/Cu SAA NPs to Cu (0.21 nm) (Fig. 4n).

2.3. .3. Successive reduction method

In the process of successive reduction method, also known as two-step method, first metal ions were reduced into NPs, followed by a subsequent reduction treatment of the second metal ions (Fig. 3f). Pei et al. (2014) prepared Pd_1/Au SAAs supported on silica gel by the successive reduction method through the introduction and reduction of Pd $(NO_3)_2$ solution on the newly formed Au/SiO_2 for acetylene hydrogenation. Zhang et al. (2014) utilized L-ascorbic acid to reduce Au^{3+} ions into Au atoms followed with embedded on Pd nanoclusters, forming large-scale Au_1/Pd SAA NPs by a facile successive reduction method.

2.4. Summary of preparation methods

The representative preparation methods of SAAs and their advantages as well as disadvantages were summarized in Table 1. PVD route can be applied to fabricate SAAs model surface catalysts in a controllable way for fundamentally studying the activation, diffusion, and desorption of reactants. However, this method is not compatible with industrial manufacturing as a result of high equipment cost and low yield. ALD route is capable of precisely controlling the size and dispersion of particles on a substrate through the sequential and self-limiting surface reactions, which is considered as a favorable tool for large-scale synthesis of stable SAAs. ALD technology has limitations in the slow deposition rates, high equipment cost, and particular metal precursors. Wet-chemistry method is recognized as one of the most appropriate methods for industrial production of SAAs because of the easy operation. Among which, the incipient wetness impregnation method is attractive to prepare a wide variety of SAAs by the choice of loading amounts and metal species. However, it may not be suitable for the synthesis of SAAs with high metal loading due to the aggregation tendency of single metal atom into NPs. Galvanic replacement method can be employed to generate various special SAA structures, but is limited by the necessary difference of reduction potentials between two metals. Successive reduction method is capable of loading single metal atoms on the specific metal host through a consecutive reduction procedure. However, the preparation process of successive reduction method is complex and the structure of the formed SAAs is difficult to control.

3. Catalytic properties and catalyst design of SAAs

SAAs, as a class of frontier catalysts, can maximize atom efficiency to reduce the noble metal usage and show unique catalytic performances in a variety of catalytic reactions (Fig. 5). Significantly, SAAs are able to break linear scaling relationships by facile activation and weak binding, consequently exhibiting remarkable catalytic activity and selectivity. Specifically, it is of great significance for the rational design of highly efficient SAA catalysts to fundamentally understand surface structure, active sites and reaction mechanisms by theoretical calculations, advanced characterization techniques and catalytic evaluations.

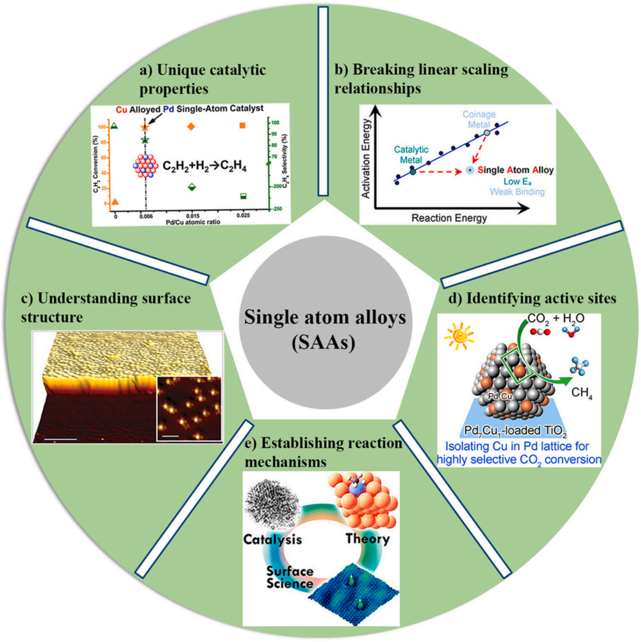

Fig. 5. Schematic illustration of properties and features of SAAs. a) SAAs exhibit unique catalytic properties derived from the maximize atom utilization and alloying effects. b) SAAs have the potential to break linear scaling relationships by facile activation and weak binding. (c) The understanding of the atomic-scale surface structure of SAAs is essential to alter both the catalytic selectivity and activity. d) The identification of active sites is helpful for optimizing and designing new catalysts. e) The establishment of mechanisms is proposed from the integration of surface science, theory, and catalysis, which is significant for developing highly efficient catalysts and determining the key steps in catalytic reactions.

(a) Reproduced with permission Pei et al. (2017). Copyright 2017, American Chemical Society. (b) Reproduced with permission Darby et al. (2018a). Copyright 2018, American Chemical Society. (c) Reproduced with permission Marcinkowski et al. (2013). Copyright 2013, Springer Nature. (d) Reproduced with permission Long et al. (2017). Copyright 2017, American Chemical Society. (e) Reproduced with permission Darby et al. (2018b). Copyright 2018, American Chemical Society.

Table 1

Summary of some representative SAAs with advantages and disadvantages of corresponding synthetic methods.

Synthetic method		Samples	Merits	Demerits
PVD route		$Pd_1/Cu(111)$; $Pd_1/Au(111)$	Simple steps	High equipment cost; Low yield
ALD route		Pd_1/Ni SAA NPs	Controllable size and dispersion	High equipment cost
Wet-chemistry routes	Incipient wetness impregnation	Pt_1/Cu SAA NPs; Pd_1/Ag SAA NPs	Easy operation; Low cost	Low yield; Long synthesis cycle
	Galvanic replacement	Pt_1/Cu SAA NPs	Special compositions and structures	Necessary difference of reduction potentials
	Successive reduction	Au_1/Pd SAA NPs	Available complex structures	Complicated steps

3.1. *Unique catalytic performances*

At present, several studies have shown that SAAs can maximize the utilization of noble metals and exhibit appealing catalytic activity and selectivity (Fig. 5a) (Pei et al., 2017). The highly diluted isolated active metal atoms have large influence on the catalytic properties of host metal. Specifically, SAAs are aimed to integrate the unique ability of single atoms and host metal derived from the synergistic effects, affording unique activity and selectivity. For example, Pt catalysts perform well in C–H activation but are prone to coking. Cu catalysts

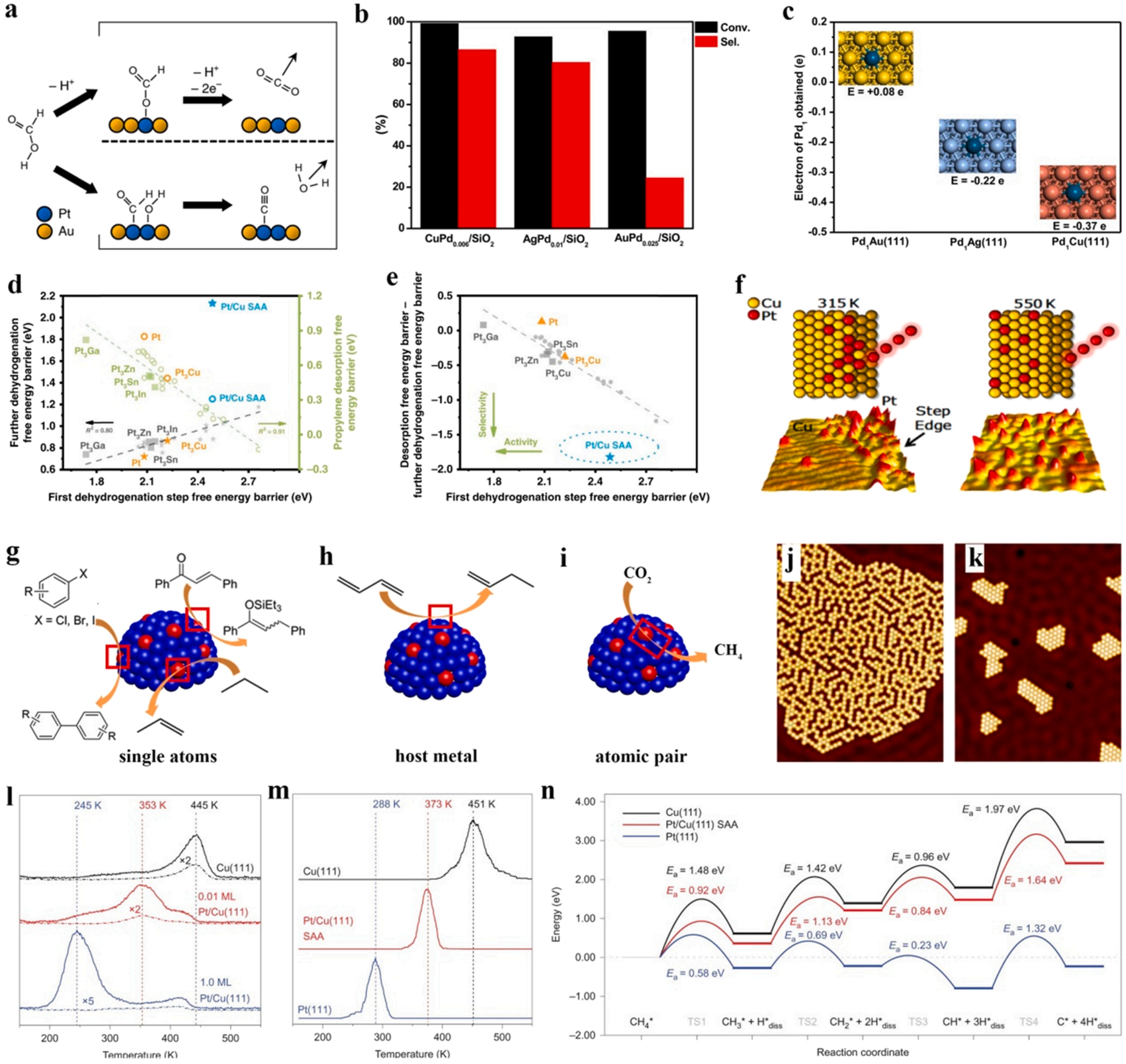

Fig. 6. (a) Description of FAOR towards the dehydrogenation pathway (top) on PtAu surfaces with single Pt sites and dehydration pathway (bottom) on PtAu surfaces with few Pt sites. (b) Acetylene conversion and ethylene selectivity at 160 °C of $CuPd_{0.006}/SiO_2$, $AgPd_{0.01}/SiO_2$, and $AuPd_{0.025}/SiO_2$ catalysts. (c) DFT calculation results of electron states of $Pd_1/Ag(111)$ SAAs, $Pd_1/Cu(111)$ SAAs and $Pd_1/Au(111)$ SAAs. (d) Scaling relationship between first dehydrogenation barrier and propylene desorption barrier/deep dehydrogenation barrier (highest barrier from di-σ propylene to C_3H_4). (e) Screening of Pt-based bimetallic catalyst for dehydrogenation of propane. (f) STM images of $Pt_1/Cu(111)$ SAAs prepared by dispersing Pt at different temperatures. The arrangement of Pt atom changes from densely packed brims/fingers at step edges at 315 K (d) to an evenly dispersed across Cu terraces at 550 K. (g) The single metal atoms isolated by host metal atoms function as active sites towards diverse catalytic reactions. (h) The host metal sites in SAAs are also regarded as the active sites for selective hydrogenation reaction. (i) The isolated metal atom in a host metal provides the atomic pair to act as the active site for CO_2 conversion into CH_4. STM images of intermediates during the reaction of CH_3I on (j) Cu(111) and (k) 0.01 ML $Pt_1/Cu(111)$ SAA surface. (l) TPR results of methane (solid lines) and ethene (dashed lines) from Cu(111) (black), 0.01 ML Pt/Cu(111) (red) and 1.0 ML Pt/Cu(111) blue) surfaces following deposition of CH_3I. 1.0 ML Pt/Cu(111) is similar to Pt(111). (m) Simulated TPR of methyl-covered Cu(111) (black), Pt/Cu(111) SAA (red) and Pt(111) (blue). (n) Energy landscape for the full dehydrogenation of adsorbed CH_4* on Cu(111) (black), Pt/Cu (111) SAA (red) and Pt(111) (blue).

(a) Reproduced with permission Duchesne et al. (2018). Copyright 2018, Springer Nature. (b, c) Reproduced with permission Pei et al. (2017). Copyright 2017, American Chemical Society. (d, e) Reproduced with permission Sun et al. (2018). Copyright 2018, Springer Nature. (f) Reproduced with permission Lucci et al. (2014). Copyright 2014, American Chemical Society. (j-n) Reproduced with permission Marcinkowski et al. (2018). Copyright 2018, Springer Nature.

facilitate C–C coupling to avoid coking whereas suffer from high C–H activation barrier. Marcinkowski et al. (2018) prepared Pt_1/Cu SAAs as the promising catalysts for coke-resistant C–H activation by virtue of combining the accelerated C−H activation activity of Pt and the C–C coupling ability of Cu to avoid coking. Moreover, SAAs can modulate activation energy and binding strength of intermediates by ligand (electronic) and geometric (ensemble) effects between single isolated atoms and host metal, thus distinctively enhancing activity and selectivity in catalytic reactions. A ligand effect referred to the electronic configuration of single metal atoms influenced by host metal through electron transfer (Fan et al., 2020). The geometric effect is related to altering geometric configuration or diluting active metal sites by the second metal (Coq and Figueras, 2001). For instance, direct dehydrogenation of formic acid requires single Pt atom, whereas several adjacent Pt atoms are in favor of the indirect dehydration pathway (Neurock et al., 2009). Alloying single Pt atom in Au created the ensemble effect to realize remarkable selectivity towards the direct dehydrogenation of formic acid (Fig. 6a) (Duchesne et al., 2018). In addition, the alloying of single metal atom has an influence on the reactivity of neighbored Pd atoms through the ligand effect (electronic interaction) for the electrochemical oxidation of formic acid (Sui et al., 2020). Furthermore, the geometric effect created by the isolation of Pd single atoms by Cu and the electron transfer from Cu to Pd could promote the activation of H_2 and decrease the adsorption strength of ethylene to realize high selectivity to ethylene and high activity in the hydrogenation of acetylene (Pei et al., 2017). The DFT results showed that electron was transferred from Cu or Ag to Pd and leaded to negatively charged Pd atoms, which accounted for higher selectivity to ethylene of Pd_1/Ag(111) SAAs or Pd_1/Cu(111) SAAs than that of Pd_1/Au(111) SAAs (Fig. 6b, c).

3.2. Breaking linear scaling relationships

The BEP relationship unravels a linear relationship between the activation energy and the reaction energy of a chemical reaction (van Santen et al., 2010). Thus, there is a compromise between low activation barrier and weak binding in an active site (Abild-Pedersen et al., 2007). Frequently, the promotion of the activity for target products accompanies some side reactions, which ultimately give rise to the decreased selectivity. Owing to the synergistic effects of isolated single atoms and host metal for facile activation and weak binding, SAAs are capable of escaping the restraint of the BEP relationship and consequently show an excellent catalytic performance (Fig. 5b) (Darby et al., 2018a, 2018b). For example, Pt lowered the C–H activation barrier with an accelerated activity over Cu. However, Pt possessed strong binding of CH_x intermediates for coking compared to Cu (Marcinkowski et al., 2018). DFT calculation revealed that Pt_1/Cu SAAs integrate low C–H activation barriers with weak adsorption of CH_x intermediates for resisting coke formation, which breaks the BEP relationship on pure transition metal. Besides, Pt_1/Cu SAAs achieve simultaneous enhancement of propylene selectivity and propane conversion during propane dehydrogenation at high temperatures (Sun et al., 2018). The activity of propane dehydrogenation was represented by the first dehydrogenation barrier, and the selectivity was evaluated by the difference between propene desorption barrier and further dehydrogenation barrier. Commonly, low dehydrogenation barrier for high propane dehydrogenation activity accompanies with strong propylene adsorption towards low propylene selectivity as a result of the scaling relationship on Pt-based alloys (Fig. 6d). However, Pt_1/Cu SAAs possess a reasonably low dehydrogenation barrier for a high activity and exhibit high propylene selectivity due to the weak binding of propylene and high further dehydrogenation barrier (Fig. 6e). Hence, SAAs show high potential to break the BEP relationship for the enhanced catalytic performance.

3.3. Understanding surface structure

The surface stoichiometry and geometry of SAAs have great effect on the surface chemistry due to the reactivity differences of metals in SAAs, which ultimately modulate catalytic activity and selectivity. The understanding of surface structure of SAAs provides a platform to study alloying effect and structure–property relationship. The investigation of surface structure of SAAs include structural formation under different experimental condition, structural influence on the activity and selectivity, structural change during reaction process (Fig. 5c) (Marcinkowski et al., 2013). First of all, STM are commonly used to investigate the local atomic structure of SAAs in the morphology, distribution and coverage under experimental conditions. Lucci et al. (2014) used STM to characterize the local atomic arrangement of Pt atoms in the submonolayer of Cu(111). They demonstrated that the arrangement of Pt in the surface was controlled by the alloying temperature of Cu(111) and showed that Pt atoms were in high dispersion at high temperature. Pt atoms were localized in regions at step edges with dense Pt brims and fingers at 315 K. At higher temperature (500 K), the isolated Pt atoms were well dispersed in Cu terraces without the appearance of Pt brims and fingers and a visible interface between the Pt brims and Cu terraces (Fig. 6f). Then, the atomic structure of the SAAs surface can alter both the reaction selectivity and reactivity. Lucci et al. (2015b) investigated the relationship of H_2 activation, spillover, and release to the surface structure of Pt_1/Cu SAAs. Using STM, they observed that the H atoms moved from Pt atom site to Cu surface, revealing a spillover mechanism of H atoms. Notably, carbon monoxide (CO), a common catalyst poison, was used as the probe molecule for investigating the surface structure and atomic dispersion of SAAs. The surface atomic structure of, and CO binding on Ni_1/Cu SAAs (Patel et al., 2019) and Ru_1/Cu SAAs (Hannagan et al., 2020b) was deciphered through an integration of characterization methods, which demonstrated the existence of isolated metal atoms and weak binding of CO on SAAs. Specially, Ouyang et al. (2021) demonstrated that CO can transition a PdAu alloy between a SAA structure and a Pd cluster structure from the combined DFT calculations and experiments. These two catalyst structures exhibited different selectivity for the dehydrogenation of ethanol. The SAA phase was selective to form acetaldehyde and hydrogen, while Pd clusters tended to form a series of catalytic products. Furthermore, the reaction conditions often cause the change of surface structure, composition and electronic states of catalysts, thus affecting the reactivity. Simonovis et al. (2018) used *in-situ* characterization techniques to study the surface change of Pt_1/Cu SAAs influenced by CO under reaction conditions. Liu et al. (2020) also exploited the surface reconstruction of Cu_1/Au SAAs under electrochemical conditions by the combined characterization technologies, theoretical simulation and DFT calculations.

3.4. Identifying active sites

Active sites are entities on the surface of catalyst for molecular binding and reaction occurrence. A deep understanding of the properties of active sites is conducive to improve the existing catalysts and design new catalysts with an excellent performance (Chen et al., 2017). However, accurate identification of the active sites is challenging owing to the quantum size effect (Lopez-Acevedo et al., 2010) and geometric effect (Nørskov et al., 2008). The clear and uniform structure of SAAs facilitates the identification of active sites in a series of reactions examined through DFT calculations, *in-situ* characterization techniques and catalytic reaction evaluations (Fig. 5d). Typically, the single metal atoms isolated by host metal atoms function as active sites towards diverse catalytic reactions (Fig. 6g). For example, the individual, isolated Pt atoms dispersed in Cu NPs served as promising active sites for dehydrogenation of alkane at high temperatures from the DFT calculations and practical catalytic reaction (Sun et al., 2018). The isolated single Pd atom in Au NPs served as the active site for Ullmann coupling of aryl chlorides (Zhang et al., 2014). The single Pd atoms in alloy NPs functioned as the main active site for effective hydrosilylation of α,β-unsaturated ketones and alkynes (Miura et al., 2017). In addition, the host metal sites are also regarded as the active sites for selective reaction after alloying with single metal atom (Fig. 6h). Lucci et al. (2015a) suggested that Cu sites were active sites over the $Pt_1/Cu(111)$ SAAs for the selective hydrogenation of butadiene. Furthermore, the isolated metal atom in a host metal provides the atomic pair to act as the active site for catalytic reaction (Fig. 6i). Long et al. (2017) reported that a Cu−Pd atomic pair in Cu_1/Pd SAAs functioned as active sites for photocatalytic reaction of CO_2 into CH_4.

3.5. Establishing reaction mechanisms

The establishment of intrinsic reaction mechanisms is of particular interest in developing highly efficient catalysts and identifying the rate-determining steps involved in reactions (Li et al., 2020). Compared with traditional metal NP catalysts, the well-defined active sites and uniform coordination environments of SAAs are beneficial for the theoretical modeling and simulation on reaction parameters such as energy barrier, absorption strength, and transition states. The combined experimental data and theoretical calculation provide a platform to well elucidate reaction mechanisms for the rational design of high-performance SAA catalysts (Fig. 5e) (Darby et al., 2018b). For example, Marcinkowski et al. (2018) proposed the reaction mechanism of C–H activation on Pt_1/Cu SAAs by virtue of surface science and simulations. Surface science allows measuring the surface reactivity and selectivity. The STM images of reaction intermediates and temperature programmed reaction (TPR) of methane evolution suggested that $Pt_1/Cu(111)$ SAAs activated C–H bonds in methyl groups at lower temperature than Cu and avoided coking via C–C coupling (Fig. 6j–m). DFT calculation is used to calculate the adsorption energy, activation barrier, transition states and reaction intermediates, which usually plays a great role in establishing reaction mechanisms (Zhou et al., 2021). Compared to Pt(111) and Cu(111), $Pt_1/Cu(111)$ SAAs possess intermediate barriers for C–H activation from DFT studies (Fig. 6n). Dehydrogenations of CH_x intermediates for coking formation are endothermic on Pt_1/Cu SAAs and Cu(111), while it is exothermic on Pt(111). The combined simulations and surface science illustrated that $Pt_1/Cu(111)$ SAAs can activate C–H bonds with enhanced activity over Cu and avoid coking observed on Pt. Besides, Liu et al. (2019) utilized the combined catalysis-surface science-theory approach to study the selective hydrogenation of 1-hexyne to 1-hexene over Pd_1/Au SAA catalysts.

3.6. Summary of catalytic properties and catalyst design of SAAs

Recently, SAAs have been widely studied in many catalytic reactions because SAAs can maximize atom utilization from single atom and modulate catalytic properties from alloying effect. For instance, SAAs exhibit remarkable catalytic performance derived from the synergistic effects between single atom and host metal. Besides, the existing electronic and geometric effects are able to alter the whole activity and selectivity towards reactions. It is noteworthy that SAAs hold the promise to break linear scaling relationships due to the ability of low barrier and weak bonding by SAAs, which thus simultaneously represent high activity and selectivity. Moreover, it is useful to design efficient SAA catalysts through understanding surface structure, identifying active sites and establishing reaction mechanisms. Due to the influences on the reaction selectivity and reactivity by atomic structure, it is essential to investigate the atomic-scale surface structure and even structural change of SAAs by *in-situ* technologies for designing fine catalysts. In addition, the clear and uniform structure of SAAs is advantageous for the identification of active sites in SAAs by theoretical calculations and experiments to improve the existing available catalysts and develop new catalysts. Furthermore, the well-defined active site of SAAs is beneficial to establishing reaction mechanisms from the integration of surface science, theoretical calculations, and catalytic studies, which is of great significance for the development of highly efficient catalysts and the determination of the rate-determining steps in catalytic reactions.

4. Applications in environmental catalysis of SAAs catalysts

The rapid growth of population and the development of industry and agriculture have caused a large amount of pollutant discharge and energy crisis, which have a great negative influence on human society and surrounding environment (Salthammer et al., 2018). Pollutants, such as VOCs, nitrogen oxides, carbon oxides, and sulfur oxides are emitted from industrial production processes and transportation, which cause risks and harm to both the environment and human health (He et al., 2019; Rajabi et al., 2020). Therefore, more and more efforts have been dedicated to the environmental applications for dealing with these pollutants and developing new energy (Ding et al., 2019; Perreault et al., 2015). Over the past decades, several approaches have been used to control the emissions of pollutants by absorption (Liu et al., 2019), condensation, biological degradation, and catalysis (Dai et al., 2021; Liu et al., 2020; Wang et al., 2020) (). Among which, catalysis is attractive in the elimination of environmental pollutants, development of clean energy and production of high value-added chemicals (Weon et al., 2021; Zhang et al., 2020). It is essential to design and develop highly efficient and chemically stable heterogeneous catalysts with tuneable structures and abundant active sites for environmental applications (Hao et al., 2021). Owing to the maximum atom efficiency as well as the unique catalytic properties, SAAs exhibited remarkable performance in the environmental catalysis. SAAs are effective in the catalytic elimination of pollutants into harmless products to control the emission of pollutants. At the same time, SAAs can catalytically transform pollutants especially VOCs into clean energy and high value-added products. In the following section, we discussed the SAAs catalysts towards different air pollutants with applications in production of clean energy and valuable chemicals as well as catalytic elimination of pollutants. SAAs exhibited excellent performances in many important reactions such as (electrochemical) oxidation of VOCs, dehydrogenation of VOCs, CO_2 conversion, NO_x reduction, CO oxidation, and SO_3 decomposition (Table 2).

4.1. Applications in production of clean energy and valuable chemicals

Large emission of pollutants will cause threat and irreversible harm to environment and human health (Tsai, 2018). It is a prospective strategy to utilize effective catalysts for the catalytic conversion of pollutants into clean energy and fine chemicals. Owing to the unique catalytic properties as well as electronic and geometric structures of SAAs, SAAs exhibited excellent performance for the conversion of pollutants into clean energy and valuable chemicals in diverse reactions such as electrochemical oxidation of alcohols and formic acid, selective oxidation of alcohols, dehydrogenation of alcohols and alkanes as well as carbon dioxide conversion.

4.1.1. Electrochemical oxidation of alcohols

Alcohols such as methanol, ethanol, and 2-propanol are commonly used as solvents and reactants in some industrial processes (Fiorenza et al., 2015). A large number of alcohols are emitted from the industrial production and waste. Long-term exposure to short-chain alcohols may cause several harms to human health such as irreversible toxicity, inhalation and skin hazard, central nervous system disorder, and oral exposing risk (Kamal et al., 2016). It is noteworthy that alcohols are also used as potential green fuels or act as raw materials for the production of energy and valuable chemicals (Anke et al., 2019). Importantly, SAAs showed excellent performances in the catalytic transformation of alcohols into valuable products and clean energy (Cordon et al., 2021).

The electrochemical oxidation of alcohols is a versatile and environmentally friendly process, which provides electrochemical power energy for potential portable applications (Siwal et al., 2019). Methanol and ethanol are two commonly used fuels becuse they are well kown for producing high power densities in direct alcohol fuel cells with platinum-based catalysts (Alias et al., 2020). However, the platinum surface is easily poisoned by the adsorbed intermediates (CO) during the

Table 2
Summary of SAA catalysts for applications in environmental catalysis.

Applications	SAA Catalysts	Catalytic activity	Stability	References
Electrochemical oxidation of alcohols	Ni_1/Pt SAAs (nanowires)	mass activity of 7.93 ± 0.45 A mg_{Pt}^{-1} at 0.816 V (MOR) mass activity of 5.60 ± 0.27 A mg_{Pt}^{-1} at 0.785 V (EOR)	no obvious change for 3600 s at 0.65 V	(Li et al., 2019)
	Ru_1/Pt SAAs (nanodendrites)	mass activity of 1.14 A mg_{Pt}^{-1} (MOR)	maintain 60% of the initial value after 6500 cycles	(Zhang et al., 2020)
	$PtBi@PtRh_1$ (nanoplates)	mass activity of 13020 mA $mg^{-1}{}_{Pt+Rh}$ at the peak potential (EOR)	maintain 57.2% of the initial value for 20000 s at 0.6 V	(Luo et al., 2021)
	Bi_1/Pd SAAs (aerogels)	mass activity of 5.74 A mg_{Pd}^{-1} (EOR)	–	(Wang et al., 2021)
Electrochemical oxidation of formic acid	Pt_4Au_{96} NPs (single Pt sits)	mass activity of 3.77 mg_{Pt}^{-1} at 0.6 V	maintain 70% of the initial value after 1500 cycling	(Duchesne et al., 2018)
	Pt_1/Au NPs	mass activity of 10.80 A mg_{Pt}^{-1}	slight decay for 10 h at 0.4 V	(Xi et al., 2017)
	Pt_1/ATO SAAs	mass activity of 3.35 A mg_{Pt}^{-1}	0.59 A mg_{Pt}^{-1} for 1800 cycles	(Kim et al., 2018)
Selective oxidation of alcohols	Pd_1/Au SAA NPs	over 99% selectivity to acetone	–	(Wrasman et al., 2018, 2020)
Dehydrogenation of alcohols	Pt_1/Cu SAA NPs	100% selectivity of formaldehyde	keep stable at 230 °C up to 16 h	(Shan et al., 2016)
	Pt_1/Cu SAA NPs	nearly 100% selectivity of acetaldehyde	–	(Wang et al., 2018)
	Ni_1/Cu SAA NPs	closely 100% selectivity of acetaldehyde	2% drop for 43 h at 250 °C	(Shan et al., 2017)
	Ni_1/Cu SAA NPs	100% selectivity of acetaldehyde	–	(Shan et al., 2018)
	Ni_1/Au SAA NPs	nearly 100% selectivity of acetaldehyde	remain 30% at 250 °C for 50 h	(Giannakakis et al., 2018)
Dehydrogenation of alkanes	Pt_1/Cu SAA NPs	activate C–H bonds in lower temperature	without deactivation for at least 52 h at 400 °C	(Marcinkowski et al., 2018)
	Pt_1/Cu SAA NPs	propylene formation rate of 10.6 mol g_{Pt}^{-1} h^{-1}, 90% selectivity to propylene at 13.1% conversion	slightly decrease after 120 h	(Sun et al., 2018)
	$PtGa\text{-}Pb/SiO_2$ (single Pt sits)	> 30% conversion of propane, > 99.6% selectivity of propylene	no deactivation at 600 °C for 96 h	(Nakaya et al., 2020)
Carbon dioxide conversion	Cu_1/Pd SAA NPs (photocatalysis)	CH_4 selectivity of 96% with a formation rate of 19.6 μmol g_{cat}^{-1} h^{-1}	stable in a continuous 20 h test	(Long et al., 2017)
	Cu_1/Au SAAs (CO_2RR)	$FE_{(co)}$ of nearly 100% (−0.4 to −0.9 V)	a negligible decay over 40 h	(Zhao et al., 2021)
	Bi_1/Pd SAAs (CO_2RR)	$FE_{(co)}$ of 90.5% at a overpotential of 290 mV in an H-type cell; $FE_{(co)}$ of 91.8% at a overpotential of 200 mV in gas diffusion flow cells	stable for 10 h at −0.5 V	(Xie et al., 2021)
Nitrogen oxides reduction	Pd_1/Cu SAAs	complete conversion of NO to N_2	stable for 30 h at 175 °C	(Xing et al., 2019)
	Rh_1Co_3/CoO SAAs	N_2 selectivity of 100% at a temperature as low as 110 °C	remain constant within 168 h	(Zhang et al., 2015)
	$Ir_1/Ni(110)$ SAAs	N_2 selectivity > 90% at 47 °C and 100% at T ≥ 67 °C	–	(Wen et al., 2019)
Carbon monoxide oxidation	Pd_1/Au SAA NPs	full conversion at 320 °C	no deactivation for 20 h at 250 °C	(Luneau et al., 2019)
Sulfur oxides decomposition	Ag_1/Pt SAAs	lower the activation barrier for S–O bond breaking	–	(Nigam and Majumder, 2018)

MOR-methanol oxidation reaction, EOR-ethanol oxidation reaction, CO_2RR-CO_2 reduction reaction, FE(co)-CO Faraday efficiency

reaction (Fadzillah et al., 2019). The addition of second metal into the electrocatalyst modifies the electronic structure or produces the oxidized species at a lower potential through the electronic effect and bifunctional effect (Kaur et al., 2021). Similarly, through the dispersion of highly diluted metal atoms on conductive metal supports, SAAs possess accessible active sites, excellent conductivity and unique electronic structures to enhance the electrocatalytic activity (Chen et al., 2018; Darby and Stamatakis, 2021). SAAs have been widely studied for the electrochemical reactions to generate energy such as methanol oxidation reaction (MOR) and ethanol oxidation reaction (EOR). Specifically, SAAs also showed highly durability in the electrochemical operating conditions. For example, single-atom nickel modified Pt nanowires (SANi-PtNWs) showed high current density and mass activity for MOR and EOR by the single-atomic tailoring the local atomic arrangement and electronic structures of the surrounding Pt atoms (Li et al., 2019). The single-atomic alloying displayed an enhanced catalytic activity for both MOR and EOR, presenting a mass activity of 7.93 ± 0.45 A mg_{Pt}^{-1} at 0.816 V and 5.60 ± 0.27 A mg_{Pt}^{-1} at 0.785 V, respectively (Fig. 7a–d). DFT calculations suggested that CO adsorption was weakened on Ni_1/Pt SAAs, hence mitigating the catalyst poisoning by CO intermediates to boost high durability. These studies demonstrated that the single-atomic alloying approach provides a universal strategy to create effective electrocatalysts for a variety of reactions.

In addition to non-noble metal, doping atomically noble or rare metal atoms in SAAs is another promising strategy to enhance electrocatalytic performance for MOR or EOR. For instance, Zhang et al. (2020) reported that highly diluted Ru atoms dispersed on Pt nanodendrites exhibited a high specific activity of 2.66 $mAcm^{-2}$, great mass activity of 1.14 A mg_{Pt}^{-1} and best stability for MOR (Fig. 7e, f). The highly diluted Ru atoms lowered the activation barrier of MOR to enhance catalytic activity without blocking the surface-active Pt sites. Luo et al. (2021) fabricated tensile-strained Rh_1/Pt SAAs by dispersing isolated Rh atoms in a tensile-strained Pt shell on intermetallic PtBi nanoplates ($PtBi@PtRh_1$). The obtained $PtBi@PtRh_1$ exhibited a high mass-activity of 5417 mA $mg^{-1}{}_{Pt+Rh}$ at 0.6 V (vs RHE) and 13020 mA $mg^{-1}{}_{Pt+Rh}$ at the peak potential for EOR in alkaline electrolyte (Fig. 7g, h). Importantly, $PtBi@PtRh_1$ exhibited high C1–pathway selectivity (24.6%), superior anti-poisoning ability, and good durability. DFT calculations revealed the synergistic effect between Rh_1 doping and tensile strain in boosting the adsorption of ethanol and intermediates and the C–C bond breaking of the intermediates. Significantly, the assembly of SAA building blocks into 3D is attractive to retain the unique properties of SAAs and maintain the large surface area as well as porous structures of 3D architectures. Wang et al. (2021) synthesized ionic liquid functionalized Bi_1/Pd SAA aerogels with the isolated Bi atoms dispersed on Pd nanowires. The Bi_1/Pd SAA aerogels exhibited a high mass activity of 5.74 A mg_{Pd}^{-1} for EOR originated from the single-atomic Bi doping and interface engineering. DFT calculations indicated that doping single Bi atoms on Pd aerogels can lower the energy barrier of the rate-determining step, leading to the enhanced electrocatalytic activity for EOR.

4.1.2. *Electrochemical oxidation of formic acid*

Formic acid (FA) not only exists in some actual industrial wastewater

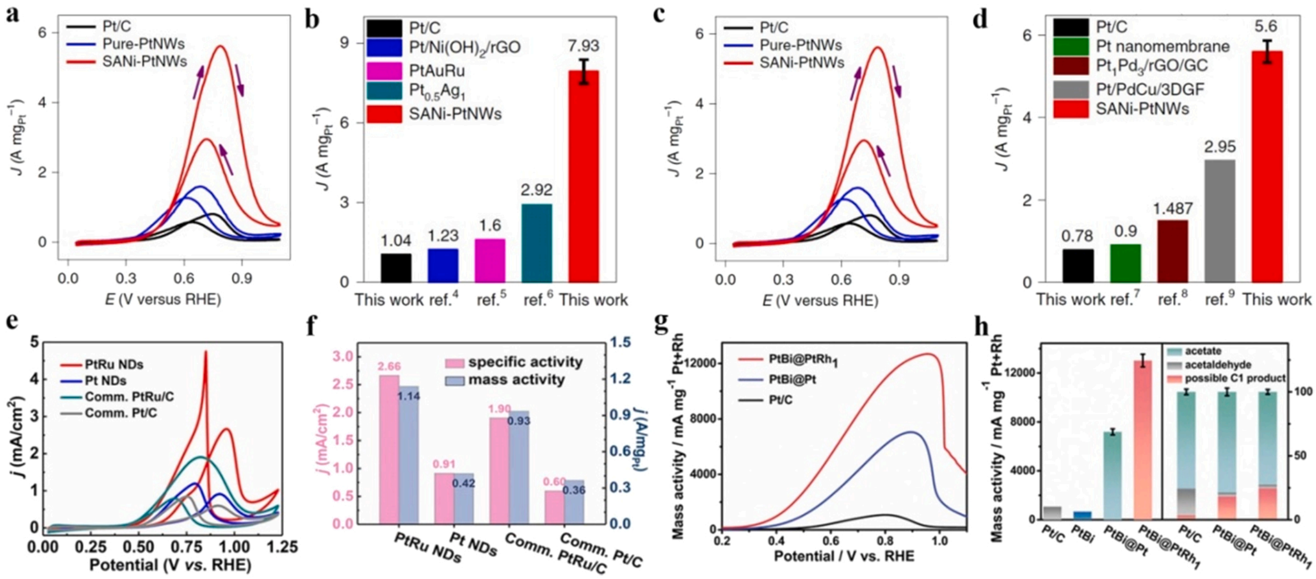

Fig. 7. MOR and EOR activities of SANi-PtNWs, pure-PtNWs and Pt/C in 1 M KOH electrolyte. (a) MOR cyclic voltammograms (CVs). (b) MOR mass activity compared with recent related work. (c) EOR CVs. (d) EOR mass activity compared with recent related work. CV studies were performed with a scan rate of 20 mV s^{-1}at 1 M methanol. (e) The MOR CVs and (f) specific and mass activity of PtRu NDs with trace Ru atoms, pure-Pt NDs, commercial PtRu/C and commercial Pt/C towards MOR. The MOR CVs were conducted in aqueous solution containing 0.5 M methanol and 0.1 M $HClO_4$ with a scan rate of 50 mV s^{-1}. (g) Positive-going CVs and (h) noble-metal mass-normalized activity and selectivity of PtBi@PtRh$_1$, PtBi@Pt, Pt/C. The EOR CVs were performed in Ar-saturated 1 M KOH and 1 M ethanol at a scan rate of 50 mV s^{-1}.

(a-d) Reproduced with permission Li et al. (2019). Copyright 2019, Springer Nature (e, f) Reproduced with permission Zhang et al. (2020). Copyright 2020, Wiley-VCH Verlag GmbH &Co. KGaA, Weinheim. (g, h) Reproduced with permission Luo et al. (2021). Copyright 2021, Wiley-VCH Verlag GmbH &Co. KGaA, Weinheim.

such as the effluents from tanners, dye workshops, and printed fabrics mills, but also is one of stable intermediates in the complete mineralization of many organic pollutants (He et al., 2004). However, formic acid is also a safe and convenient hydrogen storage fuel. The formic acid oxidation reaction (FAOR) occurs at the anode of the direct formic acid fuel cells and processes towards either direct pathway of dehydrogenation or indirect pathway of dehydration (Shen et al., 2020). In the direct pathway, FA is oxidized directly to CO_2 through dehydrogenation to formate followed by further dehydrogenation. In the indirect pathway, FA is dehydrated to CO, which is oxidized into CO_2 at high potentials (Stevanović et al., 2014). The produced CO causes the poisoning of catalysts, which is harmful to the long-term electrocatalytic applications (Hunt et al., 2016). Thus, it is necessary to develop suitable electrocatalysts for the electrocatalytic oxidation of formic acid into CO_2 and H_2 following the direct pathway to efficiently eliminate pollutants and produce clean hydrogen energy.

Recently, SAAs showed high electrocatalytic activity and selectivity towards the direct pathway in FAOR by modulating the electronic or geometric structures. Duchesne et al. (2018) reported a facile colloidal method to prepare bimetallic catalysts featured with single Pt atom embedded in Au NPs, which displayed excellent catalytic activity and selectivity for FAOR originated from the unique structures and alloying effects. The presence of several adjacent Pt sites is in favor of the production of CO towards indirect dehydration pathway, whereas the single atom Pt site promotes the formation of CO_2 and H_2 via direct dehydrogenation mechanism (Fig. 6a). As shown in Fig. 8(a), Pt/C showed a current peak at around 0.9 V, which arose from the oxidation of CO at high potential towards the indirect path. Pt_4Au_{96} with trace Pt atoms exhibited the highest mass activity of 3.77 mg_{Pt}^{-1} at around 0.6 V, following the direct path. The peak at around 0.9 V gradually disappeared with the decrease of Pt loading, indicating that PtAu alloys with highly diluted Pt atoms were resisted to CO poisoning for promoting catalytic activity. DFT calculations further demonstrated that PtAu alloys with isolated single atomic Pt sites weakly adsorbed the produced CO, which was linked to both electronic effects derived from Pt-Au bonding interactions and ensemble effects originated from discrete single atomic Pt sites. In addition, Xi et al. (2017) adopted an electrochemical method to disperse single Pt atom on Au NPs, which demonstrated an excellent catalytic performance with a high specific activity of 20.19 mA cm^{-2} and mass activity of 10.80 A mg_{Pt}^{-1} in FAOR. Moreover, Kim et al. (2018) prepared single Pt atom deposited on antimony-doped tin oxide for FAOR with high electrocatalytic activity (mass activity of 3.35 A mg_{Pt}^{-1}), selectivity, and durability. Furthermore, by using DFT calculations combined with microkinetic modelling, Sui et al. (2020) studied the FAOR on different metal$_1$/Pd(111) SAAs. The results indicated that metal$_1$/Pd(111) SAAs exhibited more excellent performance than Pd(111) and high stability for FAOR via the direct pathways. The alloying of single metal atom can not only function as the active site for FAOR but also have an impact on the reactivity of neighbored Pd atoms via charge transfer. SAAs are therefore prospective to tune the potential-determining step (PDS) of direct or indirect pathways for FAOR.

4.1.3. Selective oxidation of alcohols

Selective oxidation is also a vital process for the generation of oxygen-containing fine chemicals (Mashayekhi et al., 2014). At present, many catalysts with single active site are not capable of achieving the desired selectivity of partial oxidation over complete oxidation. SAAs hold a great promise for the enhanced performance for selective oxidation reaction from the synergetic effect between the single isolated atoms and host metal. For example, Au is beneficial to selective oxidation compared to traditional Pd or Pt catalysts due to the weak dissociative chemisorption of oxygen, especially under hydro-oxidation condition (Bravo-Suárez et al., 2008). However, the hydrogen dissociation is rate-limiting step in hydro-oxidation reaction over Au catalysts (Green et al., 2011). Wrasman et al. (2018) synthesized Pd$_1$/Au SAAs supported on TiO_2 with a controllable size and composition, which exhibited high activity and selectivity for selectively oxidizing 2-propanol to acetone with the assistance of H_2 and O_2 (Fig. 8b). The difference in acetone yield was compared between hydro-oxidation and oxidation

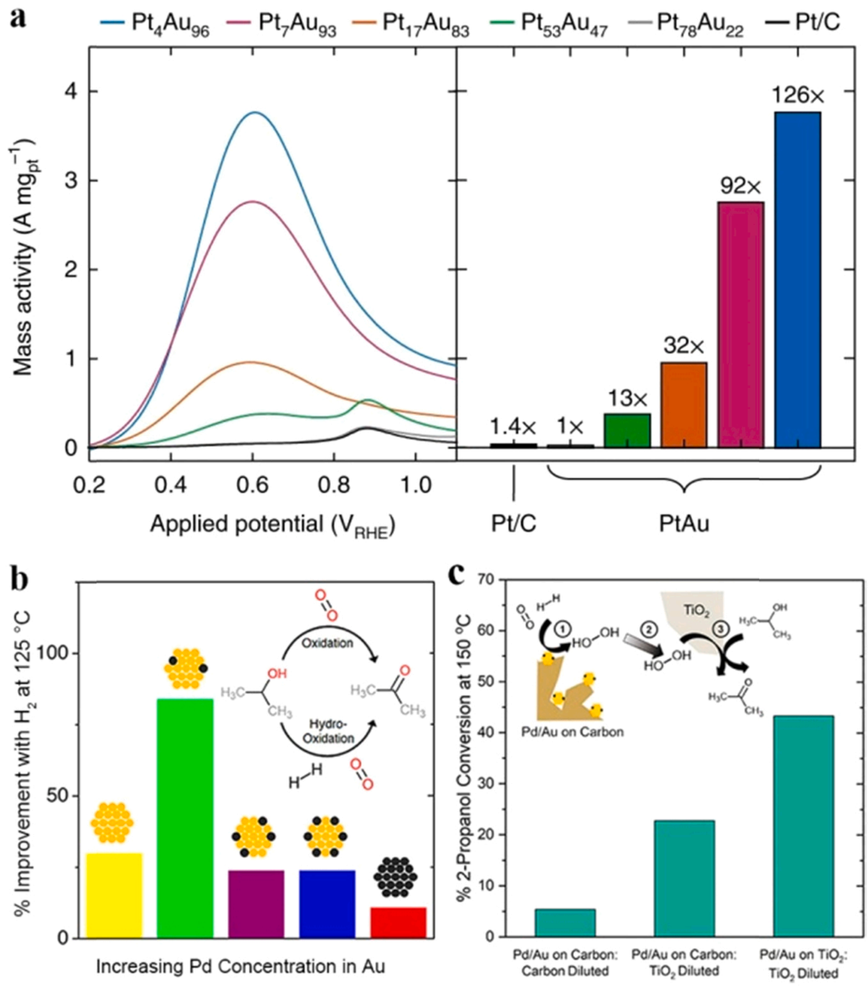

Fig. 8. (a) Mass activity of PtAu NPs tested in an electrolyte containing 0.1 M $HClO_4$ and 0.1 M formic acid (left). The corresponding peak currents were made for comparison (right). (b) The improvement of acetone yield between hydro-oxidation and oxidation conditions at 125 °C for $Pd_1/Au/TiO_2$ with the increasing ratio of Pd to Au (0, 1.4%, 4.8%, 7.0%, 100%). Inset is the schematic illustration of the different pathways from 2-propanol to acetone by oxidation (top) or a combination of hydro-oxidation (bottom). (c) Comparison of 2-propanol conversion on Pd_1/Au SAA NPs immobilized on carbon diluted with carbon, immobilized on TiO_2 diluted with TiO_2, and immobilized on carbon diluted with TiO_2 at 150 °C. Inset is the scheme description of reaction path involving the formation of H_2O_2 on Pd/Au SAA NPs supported on carbon (1), diffusion of H_2O_2 to TiO_2 (2), and the selective oxidation of 2-Propanol by H_2O.

(a) Reproduced with permission Duchesne et al. (2018). Copyright 2018, Springer Nature. (b) Reproduced with permission Wrasman et al. (2018). Copyright 2018, American Chemical Society. (c) 2 on TiO_2 (c). Reproduced with permission Wrasman et al. (2020). Copyright 2020, American Chemical Society.

conditions, showing that alloying Au with Pd single atoms exhibited higher activity and selectivity than that of either Au or Pd under hydro-oxidation conditions, as shown in a $Pd(1.4\%)/Au/TiO_2$ sample. SAAs facilitated hydrogen dissociation to form reactive hydroperoxide species from the synergistic effect between isolated Pd atoms and Au, which was benefit for selective oxidation while suppressing oxygen dissociation and total combustion. They further demonstrated Pd_1/Au SAA NPs had the capability for generating oxidants even supported on inert carbon (Fig. 8c) (Wrasman et al., 2020). The oxidants such as hydroperoxide were formed from the facile hydrogen dissociation by Pd single atoms combined with the oxygen activation without breaking the O−O bond over Au. Then hydroperoxide may diffuse through the gas phase to various metal oxides for selective oxidation of primary and secondary alcohols into their corresponding carbonyls.

4.1.4. *Dehydrogenation of alcohols*

The dehydrogenation of alcohols is the first step in partial oxidation, which is also an effective way to convert alcohols into hydrogen and aldehydes (Chidambaram and Milstein, 2013). Although Cu-based catalysts have already demonstrated great catalytic activities in the oxidative dehydrogenation of alcohols, metallic Cu is usually evaluated to be ineffective without the presence of oxygen adatoms or oxidized copper (Davies and Bowker, 2010). Alloying a trace amount of Pd, Pt, Ni atoms on Cu hosts to form unique SAAs structures can enhance the reactivity and maintain high selectivity for the non-oxidative dehydrogenation of alcohols. For instance, Boucher et al. (2013a) reported that the adsorbed water molecules on Cu(111) surface are active for the dehydrogenation of methanol to formaldehyde in the ultra-high vacuum (UHV) studies without atomic oxygen and the reaction can be facilitated by individually dispersing Pd atoms in Cu(111). The isolated Pd atoms in the copper surface promoted the dissociation of the O–H bond to form methoxy, which will be converted into formaldehyde at higher temperatures. They further extended the UHV study by $Pt_1/Cu(111)$ SAA surface to the practical application through the supported Pt_1/Cu SAA NPs in the water-catalyzed methanol dehydrogenation (Fig. 9a) (Shan et al., 2016). As shown in temperature-programmed surface reaction (TPSR) measurements, the formation of formaldehyde cannot be observed up to 400 °C in the absence of water (Fig. 9b). However, with the presence of water, the yield of formaldehyde on supported Cu NPs was far less than that on silica-supported Pt_1/Cu SAA NPs, which provided strong evidence that the reactivity of Cu was substantially boosted by alloying highly diluted Pt atoms in Cu surface for water-catalyzed dehydrogenation of methanol (Fig. 9c, d).

Additionally, SAAs also exhibited the increased activity and high selectivity for non-oxidative dehydrogenation of ethanol into acetaldehyde and hydrogen. Wang et al. (2018) found that $Pt_1/Cu(111)$ SAAs greatly increased the activity of Cu(111) for dry ethanol dehydrogenation without surface oxygen and water. The integrated STM, TPR and DFT results demonstrated that ethanol dehydrogenation on $Pt_1/Cu(111)$ SAAs was linked to dissociation of O–H bond at Pt atom sites, followed by spillover of ethoxy from Pt to Cu, and C–H activation of ethoxy at higher temperature. In addition to alloying with noble metal atoms, Shan et al. (2017) also prepared Ni_1/Cu SAAs for the non-oxidative dehydrogenation of ethanol to acetaldehyde and hydrogen under practical reaction conditions with closely 100% selectivity (Fig. 9e–h). The presence of highly diluted Ni atoms in Cu ($Ni_{0.01}Cu$ and $Ni_{0.001}Cu$)

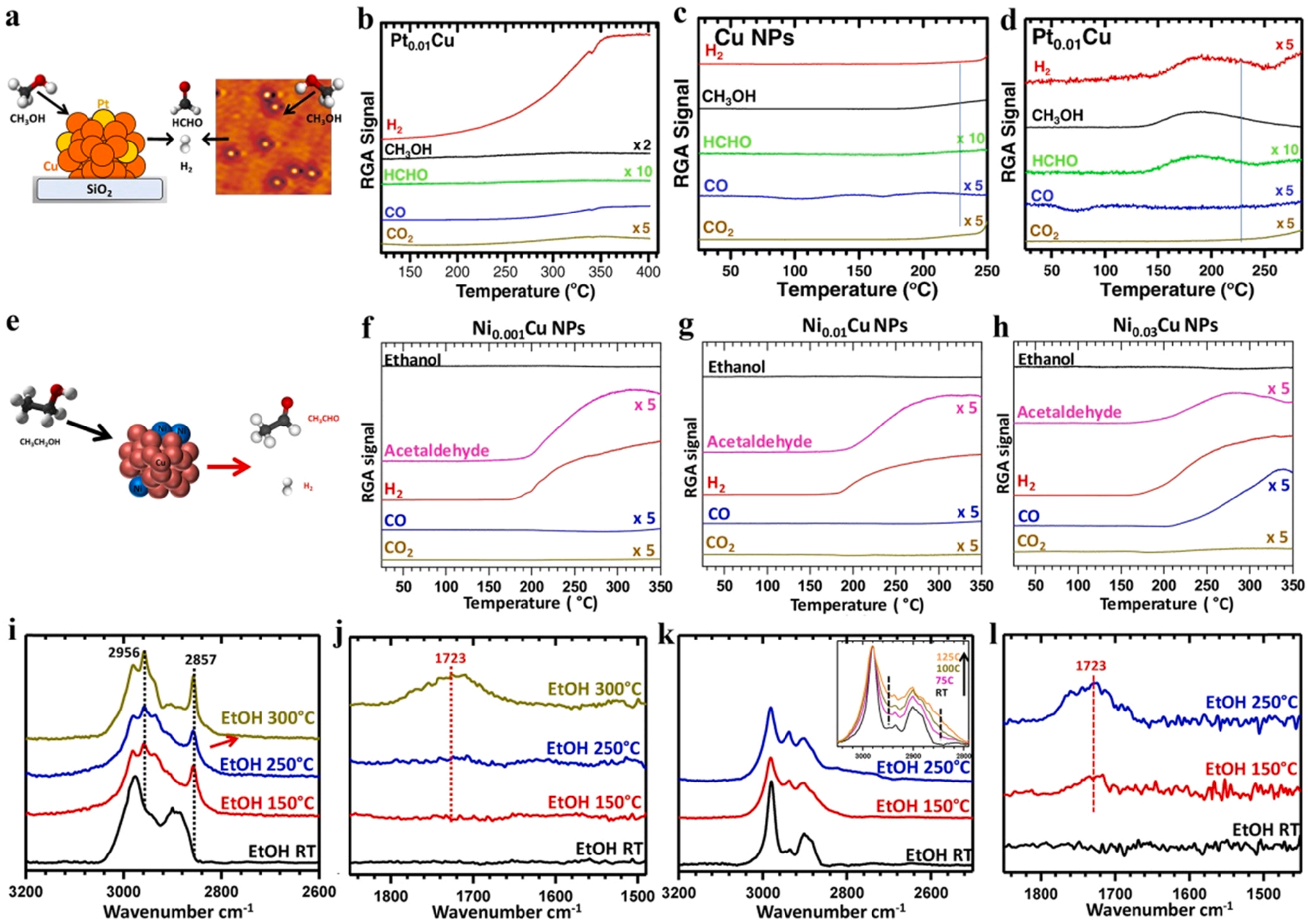

Fig. 9. (a) Schematic illustration of water co-catalyzed dehydrogenation of methanol into formaldehyde and hydrogen over Pt_1/Cu SAA NPs. (b) Temperature-programmed surface reaction (TPSR) of methanol in the absence of water $Pt_{0.01}Cu$ SAA NPs. TPSR of methanol with the existence of water on Cu NPs (c) and $Pt_{0.01}Cu$ SAA NPs. (e) Selective non-oxidative dehydrogenation of ethanol to acetaldehyde and hydrogen on Ni_1/Cu SAAs. TPSR of ethanol on $Ni_{0.001}Cu$ SAA NPs (f), $Ni_{0.01}Cu$ SAA NPs (g) and $Ni_{0.03}Cu$ SAA NPs (h) supported on silica. Diffuse reflectance infrared Fourier transform spectroscopy (DRIFTS) spectra of silica supported Cu NPs in the C-H stretching regime (i) and in the C-O stretching regime (j) after exposure to ethanol at various temperatures. DRIFTS spectra of silica supported $Ni_{0.01}Cu$ NPs in the C-H stretching regime (k) and in the C-O stretching regime (l) after exposure to ethanol at various temperatures.
(a-d) Reproduced with permission Shan et al. (2016). Copyright 2016, Elsevier. (e-h) Reproduced with permission Shan et al. (2017). Copyright 2017, Elsevier. (i-l) Reproduced with permission Shan et al. (2018). Copyright 2018, Elsevier.

dramatically improved the catalytic activity and stability against sintering. They further examined the catalytic activity of Pt_1/Cu, Pd_1/Cu, and Ni_1/Cu SAA NPs for ethanol dehydrogenation reaction through kinetic measurements and *in-situ* diffuse reflectance infrared Fourier transform spectroscopy (DRIFTS) (Shan et al., 2018). These obvious peaks at 2857 and 2956 cm^{-1} illustrated the formation of ethoxy species from dissociating O-H bond of ethanol. The appearance of new peak at 1723 cm^{-1} was linked to production of acetaldehyde at 300 °C. Clearly, the ethoxy species accumulated on Cu NPs, which cannot be observed on Ni/Cu SAA NPs at 150 °C and above (Fig. 9i, j). At the same time, acetaldehyde was formed on Ni/Cu SAA NPs occurs at a much lower temperature (150 °C) than on Cu NPs (300 °C) (Fig. 9k, l). As a comparison, the isolated Ni atoms in Cu NPs promoted the C–H bond cleavage of ethoxy species by lowering activation barrier while Pt and Pd single atom were ineffective. All these demonstrated that the C–H bond cleavage was the rate determining step in ethanol dehydrogenation over this type of catalyst. Besides, gold was applied as an alternative to copper for the selective dehydrogenation of ethanol to acetaldehyde and hydrogen (Wang et al., 2016). However, gold is not active until at temperatures above 250 °C for dehydrogenation of ethanol with high selectivity. Giannakakis et al. (2018) prepared Ni_1/Au SAAs by individually dispersed Ni atoms on Au for this reaction below 150 °C. The single Ni atom not only reduced the activation barrier with low reaction temperature, but also stabilized the catalyst morphology. Therefore, Ni_1/Au SAAs exhibited high activity, selectivity and stability for the non-oxidative ethanol dehydrogenation reaction.

4.1.5. *Dehydrogenation of alkanes*

Alkanes are important classes of organic pollutants emitted from industrial production and vehicle exhaust including ethane, propane, n-hexane, n-butane, pentane, cyclopentane, cyclohexane, n-heptane, methyl cyclohexane, and n-octane (Huang and Hsieh, 2019; Song et al., 2020). Among them, many compounds have adverse effects on environment such as air, soil and water (Randazzo et al., 2020). In addtion, alkanes are also used as feedstocks for the synthesis of fine chemicals, which are beneficial for the economic and environmental application. For example, dehydrogenation of alkanes is an industrially relevant reaction to produce alkenes and hydrogen. The C–H activation is the elementary step in the dehydrogenation reaction. Normally, Pt-based catalysts perform well in this chemistry, but are limited from coke formation and high cost. Cu-based catalysts are less active due to high C–H activation barriers while show resistance to coking. Atomic dispersion of Pt atoms with high reactivity on less active Cu metal substrate can effectively avoid coking and decrease C–H activation barrier. For example, Marcinkowski et al. (2018) performed the combined simulations and surface science to investigate the C–H activation barrier on

$Pt_1/Cu(111)$ SAAs, which revealed that $Pt_1/Cu(111)$ SAAs can activate C–H bonds with enhanced activity over Cu and avoid coking observed on Pt. During the butane–deuterium isotope scrambling experiments, the supported Pt_1/Cu SAA NPs converted butane to deuterated butane at 250 °C whereas the Cu NPs were only active at temperatures higher than 500 °C, which demonstrated that the activity of C–H activation was greatly enhanced by adding single isolated Pt atoms into the Cu surface (Fig. 10a). At the same time, the activity of Pt NPs dramatically decreased after several reactions (Fig. 10b). The Pt_1/Cu SAA NPs maintained a high activity and exhibited high stability against coking for 52 h at 400 °C in the dehydrogenation of butane to butene (Fig. 10c).

Moreover, Sun et al. (2018) developed a Pt_1/Cu SAA NP catalyst for catalytic dehydrogenation of propane with excellent activity and selectivity into propylene. The C–H activation began at about 188 °C on Pt NPs, 204 °C on Pt_1/Cu SAA NPs, and 298 °C on Cu NPs, respectively (Fig. 10d). The catalytic activity of Pt_1/Cu SAA NPs was higher than that of Cu NPs for dehydrogenation of propane. During the reaction, the propylene formation rate rapidly decreased for Pt NPs after 12 h on stream at 520 °C. As a contrast, Pt_1/Cu SAA NPs maintained the same activity for 12 h on stream with a slight decrease even after 120 h on stream (Fig. 10e, f). Sun et al. (2021) studied the origin of catalytic performance of propane dehydrogenation and coke formation for Pt_1/Cu SAAs by DFT calculations and kinetic Monte Carlo simulations. The high selectivity of propylene for Pt_1/Cu SAAs was demonstrated from the enhanced propylene formation and the high energy barrier for deep dehydrogenation. The coke formation mainly originated from the deep dehydrogenation on Pt_1/Cu SAAs, which was different from C−C bond cracking on Pt. Furthermore, single Pt atoms included in intermetallic structures is a promising strategy to maintian high activity and high thermal stability. Nakaya et al. (2020) developed PtGa-Pb/SiO_2 catalyst for efficient propane dehydrogenation, in which Pt_3 sites were selectively blocked by Pb deposition while the single-atom Pt_1 remained active. During the process of propane dehydrogenation, PtGa catalyst showed 40% conversion of propane and 99.1% selectivity of propylene at the initial 0.5 h, while the conversion gradually decreased within 50 h (Fig. 10 g, h). In contrast, PtGa-Pb/SiO_2 catalyst with single Pt atoms exhibited > 30% conversion of propane and > 99.6% selectivity of propylene at 600 °C for 96 h with outstanding stability (Fig. 10i).

DFT calculations and theoretical modeling were also utilized for the rational design of SAA catalysts. Hannagan et al. (2021) carried out

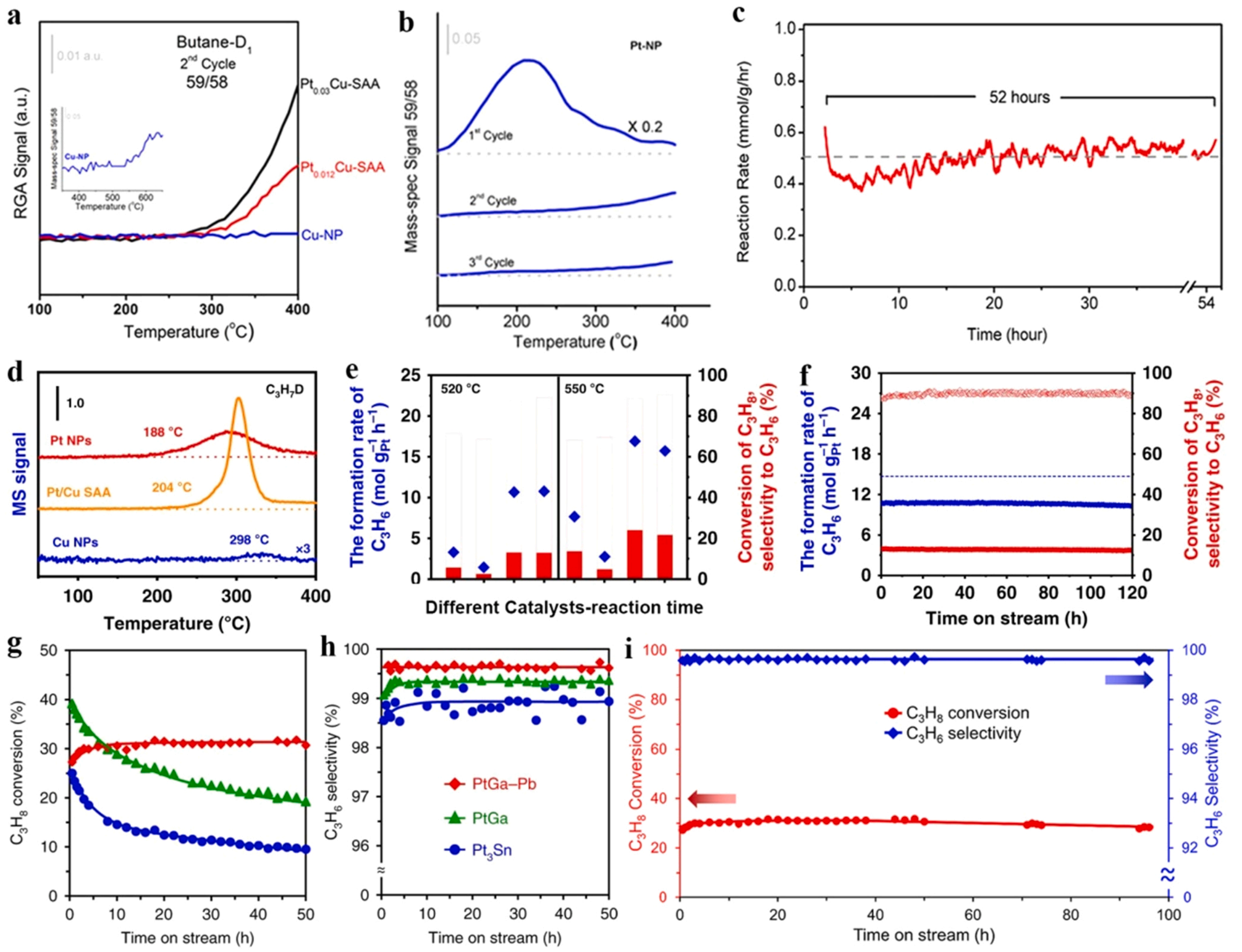

Fig. 10. (a) Butane–deuterium isotope scrambling (B–D scrambling) on $Pt_{0.03}Cu$ SAA NPs, $Pt_{0.01}Cu$ SAA NPs, and Cu NPs. Inset is the studies on Cu NPs at temperature high than 350 °C. (b) B-D scrambling on Pt NPs for different cycles. (c) The stability test for the dehydrogenation of butane on $Pt_{0.01}Cu$ SAA NPs at 400 °C for 54 h. (d) Signals of C_3H_7D on $Pt_{0.3}/Al_2O_3$, $Pt_{0.1}Cu_{10}/Al_2O_3$ and Cu_{10}/Al_2O_3 for propane–deuterium (P-D) scrambling. (e) Catalytic performances of Pt-based catalysts with different reaction time at 520 °C and 550 °C. From left to right, it referred to $Pt_{0.1}$-20 min, $Pt_{0.1}$-12 h, $Pt_{0.1}Cu_{10}$-20 min and $Pt_{0.1}Cu_{10}$-12 h. (f) The stability test on $Pt_{0.1}Cu_{10}/Al_2O_3$ at 520 °C for 120 h. Catalytic performances of propane conversion (g) and propylene selectivity (h) for propane dehydrogenation catalyzed by PtGa/SiO_2, PtGa–Pb/SiO_2, and Pt_3Sn/SiO_2. (i) Long-term stability test for propane dehydrogenation on PtGa-Pb/SiO_2 at 600 °C.

(a-c) Reproduced with permission Marcinkowski et al. (2018). Copyright 2018, Springer Nature. (d-f) Reproduced with permission Sun et al. (2018). Copyright 2018, Springer Nature. (g-i) Reproduced with permission Nakaya et al. (2020). Copyright 2020, Springer Nature.

first-principle calculations and indicated that alloying single rhodium atoms in copper surface can decrease the C-H bond activation energy. The combined simulations and surface science experiments revealed that Rh_1Cu SAAs exhibited high activity, high selectivity and high coke-resistance for the dehydrogenation of propane into propene and hydrogen. In addition, through using both DFT calculations and microkinetic modeling, Zhang et al. (2021) evaluated the activity and selectivity of ethane dehydrogenation to ethylene over several SAA catalysts by desorption energy of C_2H_4 and adsorption energy of C_2H_5, respectively. With the lowering desorption energy of C_2H_4, the activity of ethane dehydrogenation to C_2H_4 decreased. At the same time, the selectivity to C_2H_4 increased with the decreasing adsorption energy of C_2H_5.

4.1.6. *Carbon dioxide conversion*

A notable increase in the level of atmospheric CO_2 over the last few decades has been considered as a globally environmental issue, namely global warming (Prins, 2011). A lot of efforts have been made for the transformation of CO_2 into value-added chemicals, which is a promising strategy to fulfill energy demands and reduce pollutant emissions. (Aresta et al., 2014; Gao et al., 2020). For example, it holds the potential to deal with serious global warming and energy risk through the conversion of CO_2 into fuels or valuable products via (photo-/electro-) catalytic reactions (Sun et al., 2020; Tackett et al., 2019). SAAs are capable of reducing CO_2 activation barrier and improving the activity in the catalytic conversion of CO_2 (Li et al., 2020; Mohan et al., 2021).

Firstly, photocatalysis is regarded as a promising method to address the increasingly serious energy shortage and environmental pollution due to the sustainability of solar energy. Particularly, photocatalytic conversion of CO_2 into CH_4 is an attractive approach to eliminate the emission of CO_2 and develop clean energy (Wang et al., 2020). However, it suffers from the side reactions in the generation of CO and H_2 (Roy et al., 2010). It is the key to solve this major challenge through the design of catalytic sites for CO_2 adsorption and activation (Yuan et al., 2019). Long et al. (2017) explored the isolation of Cu atoms in Pd lattice to provide a highly selective site for photocatalytic conversion of CO_2 into CH_4. Pd_7Cu_1 supported on TiO_2 as the photocatalyst realized high CH_4 selectivity of 96% with a formation rate of 19.6 μmol $g_{cat}{}^{-1}$ h^{-1} (Fig. 11a, b). The adsorption of CO_2 at a Cu−Pd pair was stronger than that at a Cu−Cu pair (−0.463 eV versus −0.308 eV), which demonstrated the Cu−Pd pair constructed by individually dispersed trace Cu atoms in Pd lattice functioned as the active site for the enhanced CO_2 adsorption (Fig. 11c, d). The surface *d* states of catalysts in SAAs were tuned by ligand and strain effects. The Cu *d*-band center of Pd_7Cu_1 was greatly higher than that of Pd_1Cu_1 (−1.161 versus −1.452 eV), suggesting the elevated CO_2 activation on SAAs (Fig. 11e, f). Hence, Cu_1/Pd SAAs provide highly active sites to enhance CO_2 adsorption and activation in the photocatalytic reaction of CO_2.

Secondly, catalytic conversion of CO_2 to CH_4 is promising strategy for CO_2 utilization. Ni is known as an attractive catalyst for CO_2 conversion with excellent selectivity towards CH_4. The doping of small amounts of metal into Ni-based catalyst can efficiently promote the catalytic performamce for CO_2 conversion. Kikkawa et al. (2020) discribed the cooperative active sites in Pt_1/Ni SAAs composed of Pt atoms and neighbored host Ni atoms for the efficient and selective hydrogenation of CO_2 into CH_4 (Fig. 11g). Mohan et al. (2021) studied the doping of single metal atom in boron-promoted Ni (NiB) to reduce CO_2 activation barrier for efficient CO_2 conversion by using computational screening. Among which, Mn_1/NiB SAAs have been demonstrated to be effective for CO_2 conversion into CH_4 originated from high CO_2 adsorption energy and low CO_2 and CO* activation barriers (Fig. 11 h). At the same time, Mn_1/NiB SAAs were also suitable catalysts for dry reforming of methane due to the lowering CO_2 and CH_4 activation barriers.

Lastly, the electrochemical CO_2 reduction reaction (CO_2RR) is of particular interest for the elimination of CO_2 and production of value-added chemicals including CO, methane, ethylene, formic acid, methanol, and ethanol (Kibria et al., 2019; Tackett et al., 2020). CO is one of the main products from electrochemical CO_2RR, which is widely used in the industrial process. Generally, the process of electrochemical CO_2RR to CO involved the adsorption of CO_2, generation and desorption of *COOH as well as desorption of *CO (Tao et al., 2018). Hydrogen evolution reaction (HER) is highly competitive with electrochemical CO_2RR due to close equilibrium potentials or strong affinity of catalysts to H atoms (Sheng et al., 2017; Zhang et al., 2014). Alloying single atom on a host metal offers an effective strategy to modulate active sites, lower energy barrier and tune adsorption behavior of intermediates, consequently promoting electrocatalytic activity and selectivity (Jiang et al., 2018). Zhao et al. (2021) prepared single copper atom dispersed on hierarchical porous gold architectures for electrochemical CO_2RR. Due to the high surface area and abundant active sites, Cu_1/Au SAA catalysts exhibited an excellent electrocatalytic performance with nearly 100%

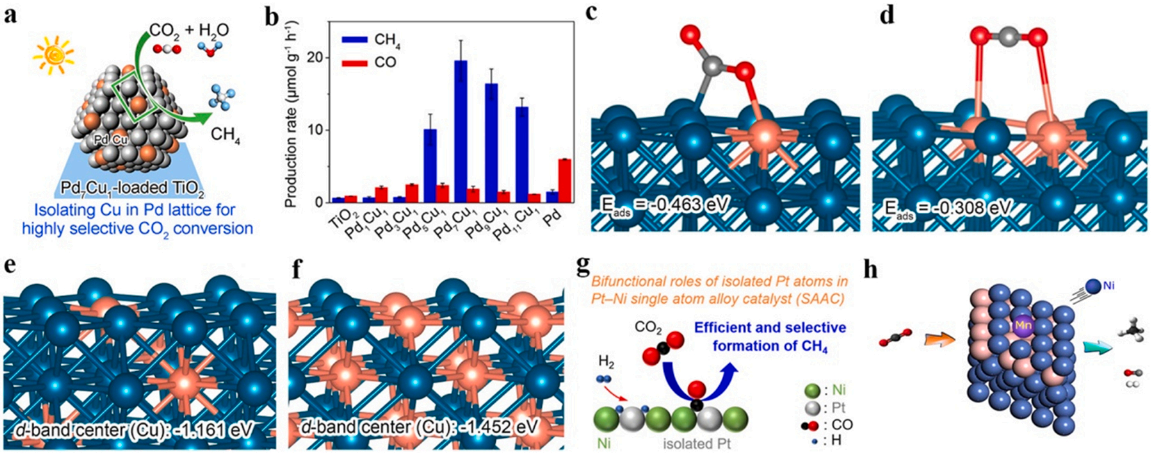

Fig. 11. (a) Illustration of photocatalytic conversion of CO_2 to CH_4 by Pd_7Cu_1/TiO_2. (b) Average production rates of CH_4 and CO in photocatalytic CO_2 reduction with H_2O by different catalysts under UV-light. The CO_2 adsorption configuration and energy at (c) single Cu atom (Cu−Pd pair), and (d) two adjacent Cu atoms (Cu−Cu pair). The structural modeling and D-band center (Cu) for (e) Pd_7Cu_1 and (f) Pd_1Cu_1 lattices. These were calculated by first-principles simulations. (g) The description of cooperative active sites composed of Pt atoms and neighbored host Ni atoms in Pt_1/Ni SAAs for selective hydrogenation of CO_2 into CH_4. (h) Illustration of single Mn atom alloyed boron-promoted Ni (Mn-NiB SAAs) as an effective catalyst for the catalytic conversion of CO_2 to CH_4 and syngas.
(a-f) Reproduced with permission Long et al. (2017). Copyright 2017, American Chemical Society. (g) Reproduced with permission Kikkawa et al. (2020). Copyright 2020, American Chemical Society. (h) Reproduced with permission Mohan et al. (2021). Copyright 2021, American Chemical Society.

CO Faraday efficiency in a wide potential range from −0.4 to −0.9 V vs. RHE and high stability over 40 h for electrochemical CO_2RR (Fig. 12a, b). *In-situ* measurements and DFT calculations indicated that the Cu−Au interface sites with substantial defects acted as the active centers to facilitate the adsorption of CO_2 and bind the *COOH intermediate. Xie et al. (2021) developed Bi_1/Pd SAA catalysts for electrochemical CO_2RR guided by DFT calculations. The DFT results revealed that the addition of single Bi atoms into Pd was benefical to reduce surface H coverage

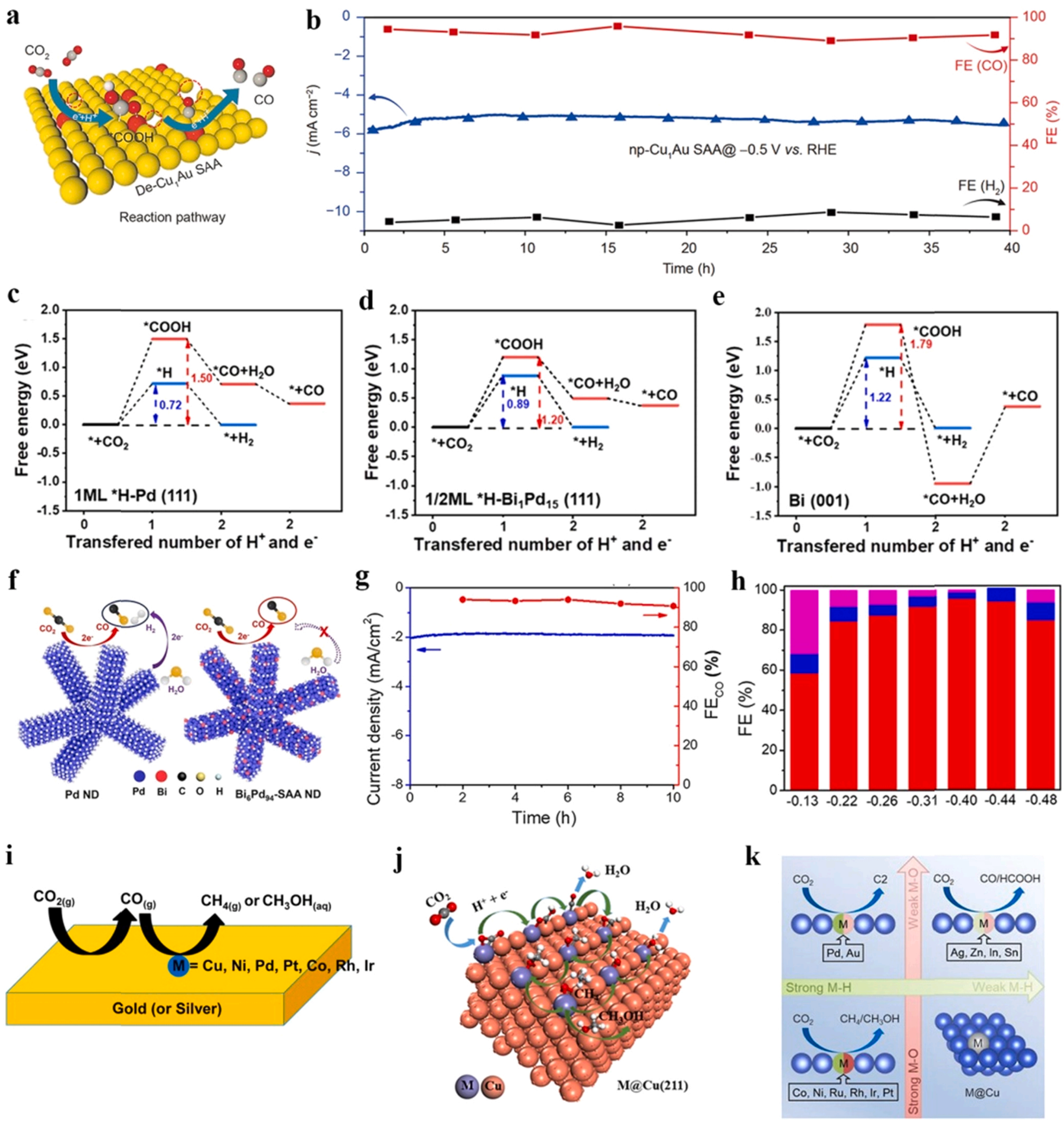

Fig. 12. Schematic illustrations of the reaction pathways of electrochemical CO_2 reduction reaction (CO_2RR) on the surface of defect-Cu_1/Au SAAs (De-Cu_1/Au SAAs). (b) Stability testing of Cu_1/Au SAA NPs. The free energy changes of hydrogen evolution reaction (HER) and CO formation for electrochemical CO_2RR on (c) Pd (111), (d) Bi_1/Pd(111) SAA and (e) Bi(001) surfaces. (f) Schematic illustration of electrochemical CO_2RR towards HER and CO formation (left) on Pd nanodendrites (NDs) and CO formation (right) on Bi_6Pd_{94} SAA NDs. (g) The current density and FE_{CO} of Bi_6Pd_{94} SAA NDs supported on carbon at − 0.5 V for 10 h in an H-type cell. (h) FEs of CO (red), H_2 (blue), and formate (pink) of Bi_6Pd_{94} SAA NDs supported on carbon for electrochemical CO_2RR in gas diffusion flow cells. (i) Schematic illustration of the proposed one-pot tandem catalytic reaction on SAA catalysts composed of isolated single atoms (Cu, Ni, Pd, Pt, Co, Rh, and Ir) embedded into the host metal surface (gold, silver). (j) Schematic description of the stepped edge on $metal_1$/Cu(211) SAAs function as the active site for electrochemical CO_2RR towards CH_4 or CH_3OH. (k) The M–H and M–O affinities in M@Cu alloys are useful descriptors in determining the selectivity of electrochemical CO_2RR.

(a-b) Reproduced with permission Zhao et al. (2021). Copyright 2021, Springer Nature. (c-h) Reproduced with permission Xie et al. (2021). Copyright 2021, Elsevier. (i) Reproduced with permission Cheng et al. (2016). Copyright 2016, American Chemical Society. (j) Reproduced with permission Feng et al. (2020). Copyright 2020, American Chemical Society. (k) Reproduced with permission Zhi et al. (2020). Copyright 2020, Elsevier.

against HER and decreased the free energy of generating *COOH intermediate for selective CO formation (Fig. 12c-e). The CO Faraday efficiency of Bi_6Pd_{94} SAA nanodendrites reached 90.5% in an H-type cell and 91.8% in gas diffusion flow cells, with overpotentials of only 290 and 200 mV, respectively (Fig. 12f–h). In addition to CO, C1 hydrocarbons are another products of electrochemical CO_2RR. Cheng et al. (2016) reported that SAAs had great potential in the electrocatalytic CO_2 reduction into C1 hydrocarbons through the combination of DFT calculations with the Poisson−Boltzmann implicit solvation model. The SAAs in the study were composed of isolated single atoms (Cu, Ni, Pd, Pt, Co, Rh, and Ir) embedded into the host metal surface (gold, silver). It was proposed that the SAAs performed as tandem catalysts in the first reduction of CO_2 to CO catalyzed by gold or silver, followed by the capture and further reduction of CO to C1 products over single metal atoms (Fig. 12i). Moreover, Feng et al. (2020) studied the activity of $metal_1/Cu(211)$ SAAs for electrochemical CO_2RR by combining DFT and microkinetic modeling. The stepped M edge was regarded as the possible active site for electrochemical CO_2RR towards CH_4 or CH_3OH (Fig. 12j). Particularly, $Ru_1/Cu(211)$ and $Fe_1/Cu(211)$ SAAs were efficiently boosting CO_2 reduction into CH_4 due to their ability in breaking the linear scaling relations of key intermediates' binding at the active sites. Furthermore, Zhi et al. (2020) used DFT calculations to explore the selectivity trends of Cu-based SAAs for CO_2 reduction by evaluating the adsorption geometry and strength, which offered a reasonable design strategy for electrocatalysts with high selectivity towards electrochemical CO_2RR. The hydrogen and oxygen affinity to the alloyed metals in Cu-based SAAs catalysts are effective descriptors in determining the selectivity of electrochemical CO_2RR (Fig. 12k).

4.2. *Applications in catalytic elimination of pollutants*

It is an emerging topic in environmental catalysis for the removal of air pollutants such as nitrogen oxides, carbon oxides, and sulfur oxides (Rezaei, 2021; Zhang et al., 2019). SAAs are particularly appealing for the elimination of these air pollutants in several ways by taking advantage of high atom utilization and alloying effect. SAAs exhibited excellent catalytic performance towards NO_x reduction, CO oxidation, and SO_3 decomposition.

4.2.1. *Nitrogen oxides reduction*

The demanded energy of the global industry is mainly produced from fossil fuel sources such as natural gas, oil, and coal. Nitrogen oxides (NO_x) are one of the key air pollutants generated during the combustion of fossil fuels (Sharif et al., 2021). It is essential to develop efficient methods for eliminating the NO_x emission owing to the adverse effect of NO_x on the environment and human health (Gholami et al., 2020). At present, platinum-group metals (PGMs) such as Pt, Pd, and Rh are known as the efficient catalysts for NO_x reduction by reducing agents such as CO, H_2, and NH_3. However, the high cost and poor thermal stability of PGMs seriously limit their further applications. The isolation of PGM atoms with an inert host metal to form SAA catalysts not only reduces the use of PGMs but also modulates the electronic and geometric structures to enhance catalytic activity and selectivity to N_2 in NO reduction. For instance, Pd_1/Cu SAAs served as an effective catalyst for NO reduction by CO at low temperature without N_2O production (Xing et al., 2019). Cu_5Pd_1/Al_2O_3 with a low amount of Pt exhibited high NO conversion and N_2 selectivity (Fig. 13a). The reaction pathway proposed by a Langmuir–Hinshelwood (L–H) model included $(NO)_2$ dimer formation, subsequent N–O breaking (N_2O formation), and N_2O decomposition (N_2 production). Kinetic and DFT studies indicated that N–O bond scission of the $(NO)_2$ dimer for N_2O formation was the rate-determining step, which was facilitated by the isolated Pd atoms. This demonstrated that the isolation of Pd atoms by Cu was the efficient catalyst for removing NO_x with low noble-metal loading.

Moreover, SAAs consisting of single metal atom and host metal offer a specific electronic structure for adsorbing or dissociating reactants to tune catalytic performance. Zhang et al. (2015) reported that the supported Rh_1/Co SAAs demonstrated a remarkable catalytic activity in the reduction of NO with CO at low temperature, arising from the strong adsorption of N_2O_2 and N_2O intermediates on Rh_1/Co SAAs sites and facile dissociation of N_2O to N_2 (Fig. 13b). The prepared Rh_1Co_3/CoO exhibited a high catalytic activity and 100% selectivity for reducing NO to N_2 at low temperature (110 °C). Except that the exploration of SAAs based on PGMs towards NO_x removal, Papanikolaou and Stamatakis

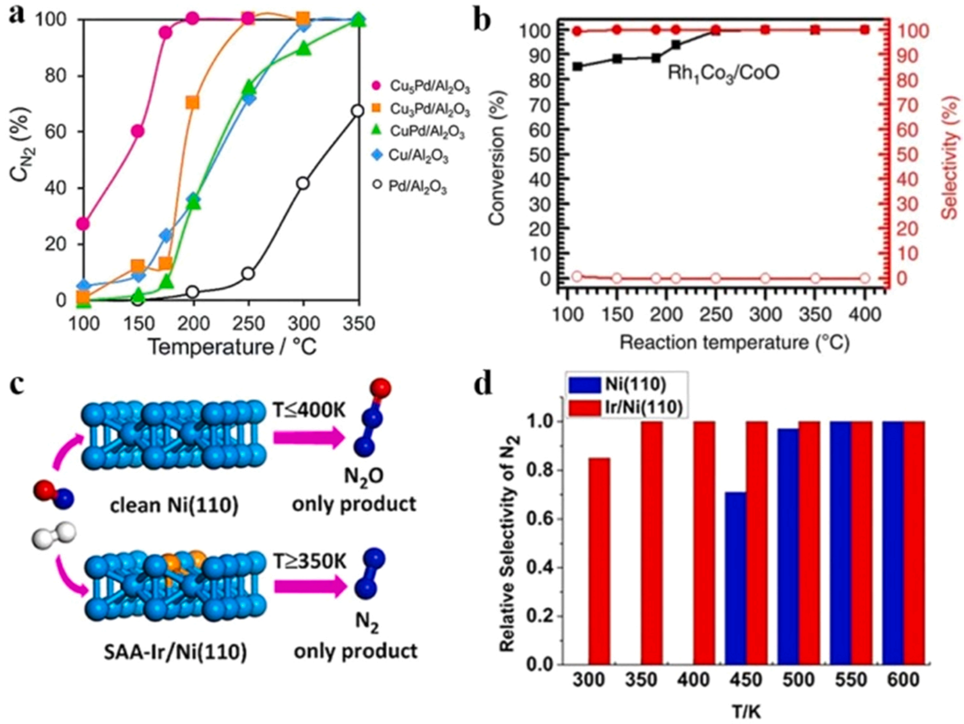

Fig. 13. (a) The reduction NO into N_2 by CO on Pd, Cu, and CuPd catalysts as a function of reaction temperature. (b) Catalytic performance of Rh_1Co_3/CoO a function of reaction temperature. Black, NO conversion; red solid circle, N_2 selectivity; red hollow circle, N_2O selectivity. (c) $Ir_1/Ni(110)$ SAAs exhibited markedly improved selectivity toward N_2 for the nitric oxide (NO) reduction by H_2 compared with Ni (110). (d) Selectivity to N_2 in NO reduction on $Ir_1/Ni(110)$ SAAs and Ni(110).

(a) Reproduced with permission Xing et al. (2019). Copyright 2019, The Royal Society of Chemistry. (b) Reproduced with permission Zhang et al. (2015). Copyright 2015, Springer Nature. (c, d) Reproduced with permission Wen et al. (2019). Copyright 2019, American Chemical Society.

(2021) reported that PGM-free $Ni_1/Cu(111)$ SAAs strengthened the binding of N_2O and promoted its dissociation for enhanced catalytic activity in the NO reduction through DFT and microkinetic modelling calculations. In addition to the utilization of CO as a reducing agent, H_2 was also applied for NO_x reduction. Wen et al. (2019) investigated NO reduction by H_2 on Ni(110) surface and $Ir_1/Ni(110)$ SAA surfaces by means of DFT calculations integrated with microkinetic modeling (Fig. 13c). The calculations showed that N_2O formation was favorable on Ni(110), whereas N_2 formation was preferred on $Ir_1/Ni(110)$ with a low energy barrier. $Ir_1/Ni(110)$ SAAs effectively boosted the high N_2 selectivity for the reduction of NO in a wide temperature range (>90% at 47 °C and 100% at $T \geq 67$ °C). Compared with Ni(110) surface with low selectivity to N_2, $Ir_1/Ni(110)$ SAAs exhibited improved selectivity at lower temperature (Fig. 13d).

4.2.2. *Carbon monoxide oxidation*

Carbon monoxide (CO) is commonly produced from the incomplete combustion of hydrocarbon fuels (Beniya and Higashi, 2019). CO is a toxic air pollutant and causes harmful effects on human health (Lu et al., 2020). CO oxidation has attracted great attention in eliminating the toxic exhaust gas emitted from automobiles (Jiang et al., 2020). CO oxidation typically follow the L–H mechanism involving O_2 and CO adsorption, followed by O_2 dissociation, and ended with the reaction of CO by adsorbed O (Jiang et al., 2014, 2018). Luneau et al. (2019) reported that Pd_1/Au SAA NPs embedded in colloid-templated silica promoted the oxygen dissociation and CO oxidation as well as showed thermally stability at high temperature for CO oxidation. Moreover, Baskaran et al. (2020) have proposed the reaction mechanism of CO oxidation over Pd_1/Au SAAs through DFT calculations. The energy profile by the calculations revealed that CO oxidation took place on Pd_1/Au SAAs towards the L–H mechanism and was a feasible process at low temperature originated from the ability of SAAs in lowering activation energy barriers. Besides, Zhang et al., 2020 investigated CO oxidation on $metal_1/Ni(111)$ SAAs such as $Rh_1/Ni(111)$, $Au_1/Ni(111)$ and $Ir_1/Ni(111)$ by DFT combined with micro-kinetic modeling. They systematically studied the rate-limiting steps, electronic effects and alloying performance of SAAs for CO oxidation. Furthermore, Filie et al. (2021) prepared atomically dispersed $Pt_1/NiFeAl$ SAAs through a topological transformation of layered-double hydroxide nanosheets. $Pt_1/NiFeAl$-600 SAAs exhibited 100% CO conversion at low temperature and a broad temperature window.

4.3.3. *Sulfur oxides decomposition*

SO_2 and SO_3 are main pollutants generated from fossil fuel combustion and other industrial process. At present, the treatment methods of SO_2 and SO_3 include absorption, chemical reaction, and biological method. The decomposition of SO_3 is the important reaction step in sulfur–iodine process, which requires high temperature and a catalyst (Nur et al., 2018). Due to the tunable geometry and chemical properties, SAAs can reduce the activation barrier and tune the binding strength to facilitate the SO_3 decomposition. The experimental use in SO_3 decomposition by SAAs has not yet been reported. The theoretical simulations have been proposed to deal with the adsorption and activation of SO_3 and intermediate. Nigam and Majumder (2018) reported that Ag_1/Pt SAAs exhibited excellent catalytic performance of SO_3 decomposition in DFT studies due to the low activation barrier and weak binding of SO_2.

5. Challenges and prospects in SAAs for environmental applications

SAAs, composed of single isolated active metal atom dispersed on host metals, have been fabricated by several methods such as PVD, ALD, wet-chemistry routes, and other methods. SAAs not only realize the low loading of noble metals to reduce the cost of catalysts, but also maximize the atom efficiency to improve the catalytic activity. Generally, SAAs exhibit remarkable catalytic performance derived from the synergistic effects between single atom and host metal. Besides, the electronic and geometric effects of SAAs are able to alter the whole activity and selectivity towards reactions. It is noteworthy that SAAs hold the promise to break linear scaling relationships due to the facile activation of reactants and weak binding of intermediates by SAAs, which thus simultaneously represent high activity and selectivity. Moreover, it is significant for the rational design of efficient SAA catalysts through understanding surface structure, identifying active sites and establishing reaction mechanisms. Due to the influences on the reaction selectivity and reactivity by atomic structure, it is essential to investigate the atomic-scale surface structure and even structural change of SAAs by *in-situ* characterization technologies for designing fine catalysts. In addition, the clear and uniform structure of SAAs is advantageous for the identification of active sites in SAAs by theoretical calculations and experiments to improve the existing available catalysts and develop new catalysts. Furthermore, the well-defined active sites of SAAs are beneficial to establishing reaction mechanisms from the integration of surface science, theoretical calculations, and catalytic studies, which is of great significance for the development of highly efficient catalysts and the determination of the rate-determining steps in catalytic reactions. Owing to the maximum atom efficiency as well as the unique features, SAAs hold a high potential for environmental catalysis towards different air pollutants with applications in production of clean energy and valuable chemicals as well as catalytic elimination of pollutants. SAAs exhibited excellent performances in many important reactions such as (electrochemical) oxidation of VOCs, dehydrogenation of VOCs, CO_2 conversion, NO_x reduction, CO oxidation, and SO_3 decomposition.

Although remarkable progress has been achieved in both synthesis and environmental catalysis of SAAs, there still are many issues that need to be addressed, which are provided below.

(1) A large-scale and controllable preparation of SAAs

The development of suitable methods for large-scale and controllable preparation of SAAs is useful but challenging for practical applications. Recently, many methods have been used for producing SAAs such as PVD, ALD, wet-chemistry routes. It remains a big challenge to realize low-cost, high-yield, and scale-up production of SAAs through a simple and universal preparation strategy.

(2) Stability of SAAs

The stability of SAAs is particularly important for practical applications, especially for long-term and high-temperature reaction. It remains a challenge to retain the single-atom characteristics during the long-term use due to the high tendency of agglomeration by high surface energy. Sometimes, the structure of SAAs is influenced by the surrounding reaction environment. Therefore, it should be considered to evaluate the single atomic active site of SAAs by using *in-situ* characterization technologies during reaction processes. It is noteworthy that selecting suitable alloy elements and improving the interaction between them are the promising strategies to enhance the stability of SAAs.

(3) More applications of SAAs in the environmental field

Applications of SAAs in the environmental field are necessary to expand to more environmental contaminants. Recent research has just focused on traditional pollutants such as VOCs and other toxic inorganic gases, while studies on the removal of water contaminant are still scarce. SAAs hold great potential in the remediation of air, water, and soil from the experimental and practical view. Next, SAAs are promising for the removal and transformation of VOCs through various catalytic reactions. For example, catalytic oxidation is a method to efficiently oxidize VOCs into water, carbon dioxide and other harmless compounds at low-temperature. Great opportunities are existed for SAAs towards various catalytic reactions in the environmental field.

(4) Complex SAA structures for specific applications

It has attracted interests in constructing complex SAA structures from SAA building blocks for target application. The complex structures provide large surface area with the abundant active sites and porous architectures with the enhanced mass/electron transfer. It is appealing to assemble SAAs building blocks into complex architectures, which can retain the unique properties of SAAs and maintain the large surface area as well as porous structures of complex architectures. Therefore, it is desirable to manufacture complex SAA structures with excellent performance for specific applications.

(5) Further studies on the active sites and reaction mechanisms of SAAs

A deep understanding of active sites and reaction mechanisms is of particular interest in improving and developing effective catalysts. The clear and uniform structure of SAAs facilitates the identification of active sites and establishment of reaction mechanisms through DFT calculations, characterization techniques and catalytic evaluations. However, SAA catalysts may undergo the dynamic restructure under reaction conditions. The *in-situ* advanced characterization technologies should be applied to investigate the structural change of active sites during catalytic reaction process, which facilitate understanding structure-property relationships and reaction mechanisms for the rational design of effective catalysts. Besides, it remains a challenge to establish theoretical model of large and complex molecules by DFT simulation. More calculations are required to evaluate the absorption and activation behaviors of large environmental pollutants on SAA catalysts for understanding catalytic mechanisms and screening suitable catalysts.

Overall, many challenges and opportunities are devoted to exploring the potential of SAAs in environmental areas in the future. We hope this review can provide a good overview for better understanding of synthetic strategies, catalytic properties, catalyst design and environmental applications of SAAs and stimulate greater interests and efforts toward their further applications.

Declaration of Competing Interest

The authors declare that they have no known competing financial interests or personal relationships that could have appeared to influence the work reported in this paper.

Acknowledgements

This work was supported by the National Natural Science Foundation of China (NO. 52100118, NO. 21777033, NO. 22176041), Science and Technology Planning Project of Guangdong Province (NO. 2017B020216003), Local Innovative and Research Teams Project of Guangdong Pearl River Talents Program (2017BT01Z032), and the Innovation Team Project of Guangdong Provincial Department of Education (NO. 2017KCXTD012).

References

Abild-Pedersen, F., Greeley, J., Studt, F., Rossmeisl, J., Munter, T.R., Moses, P.G., Skúlason, E., Bligaard, T., Nørskov, J.K., 2007. Scaling properties of adsorption energies for hydrogen-containing molecules on transition-metal surfaces. Phys. Rev. Lett. 99, 016105.

Aich, P., Wei, H., Basan, B., Kropf, A.J., Schweitzer, N.M., Marshall, C.L., Miller, J.T., Meyer, R., 2015. Single-atom alloy Pd–Ag catalyst for selective hydrogenation of acrolein. J. Phys. Chem. C 119, 18140–18148.

Alias, M.S., Kamarudin, S.K., Zainoodin, A.M., Masdar, M.S., 2020. Active direct methanol fuel cell: an overview. Int. J. Hydrog. Energy 45, 19620–19641.

Anke, S., Bendt, G., Sinev, I., Hajiyani, H., Antoni, H., Zegkinoglou, I., Jeon, H., Pentcheva, R., Roldan Cuenya, B., Schulz, S., Muhler, M., 2019. Selective 2-propanol oxidation over unsupported Co$_3$O$_4$ spinel nanoparticles: Mechanistic insights into aerobic oxidation of alcohols. ACS Catal. 9, 5974–5985.

Aresta, M., Dibenedetto, A., Angelini, A., 2014. Catalysis for the valorization of exhaust carbon: From CO$_2$ to chemicals, materials, and fuels. Technological use of CO$_2$. Chem. Rev. 114, 1709–1742.

Baptista, A., Silva, F., Porteiro, J., Míguez, J., Pinto, G., 2018. Sputtering physical vapour deposition (PVD) coatings: a critical review on process improvement and market trend demands. Coatings 8, 402.

Baskaran, S., Xu, C.-Q., Wang, Y.-G., Garzón, I.L., Li, J., 2020. Catalytic mechanism and bonding analyses of Au-Pd single atom alloy (SAA): CO oxidation reaction. Sci. China Mater. 63, 993–1002.

Bender, T.A., Dabrowski, J.A., Gagné, M.R., 2018. Homogeneous catalysis for the production of low-volume, high-value chemicals from biomass. Nat. Rev. Chem. 2, 35–46.

Beniya, A., Higashi, S., 2019. Towards dense single-atom catalysts for future automotive applications. Nat. Catal. 2, 590–602.

Boucher, M.B., Marcinkowski, M.D., Liriano, M.L., Murphy, C.J., Lewis, E.A., Jewell, A. D., Mattera, M.F.G., Kyriakou, G., Flytzani-Stephanopoulos, M., Sykes, E.C.H., 2013a. Molecular-scale perspective of water-catalyzed methanol dehydrogenation to formaldehyde. ACS Nano 7, 6181–6187.

Boucher, M.B., Zugic, B., Cladaras, G., Kammert, J., Marcinkowski, M.D., Lawton, T.J., Sykes, E.C.H., Flytzani-Stephanopoulos, M., 2013b. Single atom alloy surface analogs in Pd$_{0.18}$Cu$_{15}$ nanoparticles for selective hydrogenation reactions. Phys. Chem. Chem. Phys. 15, 12187–12196.

Bravo-Suárez, J.J., Bando, K.K., Lu, J., Fujitani, T., Oyama, S.T., 2008. Oxidation of propane to propylene oxide on gold catalysts. J. Catal. 255, 114–126.

Cao, X., Mirjalili, A., Wheeler, J., Xie, W., Jang, B.W.-L., 2015. Investigation of the preparation methodologies of Pd-Cu single atom alloy catalysts for selective hydrogenation of acetylene. Front. Chem. Sci. Eng. 9, 442–449.

Cao, Y., Guerrero-Sańchez, J., Lee, I., Zhou, X., Takeuchi, N., Zaera, F., 2020. Kinetic study of the hydrogenation of unsaturated aldehydes promoted by CuPt$_x$/SBA-15 single-atom alloy (SAA) catalysts. ACS Catal. 10, 3431–3443.

Chen, Y., Huang, Z., Ma, Z., Chen, J., Tang, X., 2017. Fabrication, characterization, and stability of supported single-atom catalysts. Catal. Sci. Technol. 7, 4250–4258.

Chen, Y., Ji, S., Chen, C., Peng, Q., Wang, D., Li, Y., 2018. Single-atom catalysts: synthetic strategies and electrochemical applications. Joule 2, 1242–1264.

Cheng, M.-J., Clark, E.L., Pham, H.H., Bell, A.T., Head-Gordon, M., 2016. Quantum mechanical screening of single-atom bimetallic alloys for the selective reduction of CO$_2$ to C1 hydrocarbons. ACS Catal. 6, 7769–7777.

Chidambaram, G., Milstein, D., 2013. Applications of acceptorless dehydrogenation and related transformations in chemical synthesis. Science 341, 1229712.

Coq, B., Figueras, F., 2001. Bimetallic palladium catalysts: influence of the co-metal on the catalyst performance. J. Mol. Catal. A-Chem. 173, 117–134.

Cordon, M.J., Zhang, J., Purdy, S.C., Wegener, E.C., Unocic, K.A., Allard, L.F., Zhou, M., Assary, R.S., Miller, J.T., Krause, T.R., Lin, F., Wang, H., Kropf, A.J., Yang, C., Liu, D., Li, Z., 2021. Selective butene formation in direct ethanol-to-C$_{3+}$-olefin valorization over Zn–Y/beta and single-atom alloy composite catalysts using in situ-generated hydrogen. ACS Catal. 11, 7193–7209.

Dai, Z., Li, D., Ao, Z., Wang, S., An, T., 2021. Theoretical exploration of VOCs removal mechanism by carbon nanotubes through persulfate-based advanced oxidation processes: Adsorption and catalytic oxidation. J. Hazard. Mater. 405, 124684.

Darby, M.T., Réocreux, R., Sykes, E.C.H., Michaelides, A., Stamatakis, M., 2018a. Elucidating the stability and reactivity of surface intermediates on single-atom alloy catalysts. ACS Catal. 8, 5038–5050.

Darby, M.T., Stamatakis, M., Michaelides, A., Sykes, E.C.H., 2018b. Lonely atoms with special gifts: breaking linear scaling relationships in heterogeneous catalysis with single-atom alloys. J. Phys. Chem. Lett. 9, 5636–5646.

Darby, M.T., Stamatakis, M., 2021. Single-atom alloys for the electrochemical oxygen reduction reaction. Chemphyschem 22, 499–508.

Davies, P.R., Bowker, M., 2010. On the nature of the active site in catalysis: the reactivity of surface oxygen on Cu(110). Catal. Today 154, 31–37.

Ding, S., Hülsey, M.J., Pérez-Ramírez, J., Yan, N., 2019. Transforming energy with single-atom catalysts. Joule 3, 2897–2929.

Duchesne, P.N., Li, Z.Y., Deming, C.P., Fung, V., Zhao, X., Yuan, J., Regier, T., Aldalbahi, A., Almarhoon, Z., Chen, S., Jiang, D.-e, Zheng, N., Zhang, P., 2018. Golden single-atomic-site platinum electrocatalysts. Nat. Mater. 17, 1033–1039.

Fadzillah, D.M., Kamarudin, S.K., Zainoodin, M.A., Masdar, M.S., 2019. Critical challenges in the system development of direct alcohol fuel cells as portable power supplies: an overview. Int. J. Hydrog. Energy 44, 3031–3054.

Fan, J., Du, H., Zhao, Y., Wang, Q., Liu, Y., Li, D., Feng, J., 2020. Recent progress on rational design of bimetallic Pd based catalysts and their advanced catalysis. ACS Catal. 10, 13560–13583.

Feng, Y., An, W., Wang, Z., Wang, Y., Men, Y., Du, Y., 2020. Electrochemical CO$_2$ reduction reaction on M@Cu(211) bimetallic single-atom surface alloys: Mechanism, kinetics, and catalyst screening. ACS Sustain. Chem. Eng. 8, 210–222.

Filie, A., Shirman, T., Aizenberg, M., Aizenberg, J., Friend, C.M., Madix, R.J., 2021. The dynamic behavior of dilute metallic alloy Pd$_x$Au$_{1-x}$/SiO$_2$ raspberry colloid templated catalysts under CO oxidation. Catal. Sci. Technol. 11, 4072–4082.

Fiorenza, R., Crisafulli, C., Condorelli, G.G., Lupo, F., Scirè, S., 2015. Au–Ag/CeO$_2$ and Au–Cu/CeO$_2$ catalysts for volatile organic compounds oxidation and CO preferential oxidation. Catal. Lett. 145, 1691–1702.

Gao, W., Liang, S., Wang, R., Jiang, Q., Zhang, Y., Zheng, Q., Xie, B., Toe, C.Y., Zhu, X., Wang, J., Huang, L., Gao, Y., Wang, Z., Jo, C., Wang, Q., Wang, L., Liu, Y., Louis, B., Scott, J., Roger, A.-C., Amal, R., He, H., Park, S.-E., 2020. Industrial carbon dioxide capture and utilization: state of the art and future challenges. Chem. Soc. Rev. 49, 8584–8686.

Gawande, M.B., Fornasiero, P., Zbořil, R., 2020. Carbon-based single-atom catalysts for advanced applications. ACS Catal. 10, 2231–2259.

George, S.M., 2010. Atomic layer deposition: an overview. Chem. Rev. 110, 111–131.

Gholami, F., Tomas, M., Gholami, Z., Vakili, M., 2020. Technologies for the nitrogen oxides reduction from flue gas: a review. Sci. Total. Environ. 714, 136712.

Giannakakis, G., Trimpalis, A., Shan, J., Qi, Z., Cao, S., Liu, J., Ye, J., Biener, J., Flytzani-Stephanopoulos, M., 2018. NiAu single atom alloys for the non-oxidative dehydrogenation of ethanol to acetaldehyde and hydrogen. Top. Catal. 61, 475–486.

Giannakakis, G., Flytzani-Stephanopoulos, M., Sykes, E.C.H., 2019. Single-atom alloys as a reductionist approach to the rational design of heterogeneous catalysts. Acc. Chem. Res. 52, 237–247.

Green, I.X., Tang, W., Neurock, M., Yates Jr., J.T., 2011. Low-temperature catalytic H_2 oxidation over Au nanoparticle/TiO_2 dual perimeter sites. Angew. Chem. Int. Ed. 50, 10186–10189.

Han, J., Lu, J., Wang, M., Wang, Y., Wang, F., 2019. Single atom alloy preparation and applications in heterogeneous catalysis. Chin. J. Chem. 37, 977–988.

Han, Z.-K., Sarker, D., Ouyang, R., Mazheika, A., Gao, Y., Levchenko, S.V., 2021. Single-atom alloy catalysts designed by first-principles calculations and artificial intelligence. Nat. Commun. 12, 1833.

Hannagan, R.T., Giannakakis, G., Flytzani-Stephanopoulos, M., Sykes, E.C.H., 2020a. Single-atom alloy catalysis. Chem. Rev. 120, 12044–12088.

Hannagan, R.T., Patel, D.A., Cramer, L.A., Schilling, A.C., Ryan, P.T.P., Larson, A.M., Çınar, V., Wang, Y., Balema, T.A., Sykes, E.C.H., 2020b. Combining STM, RAIRS and TPD to decipher the dispersion and interactions between active sites in RhCu single-atom alloys. ChemCatChem 12, 488–493.

Hannagan, R.T., Giannakakis, G., Réocreux, R., Schumann, J., Finzel, J., Wang, Y., Michaelides, A., Deshlahra, P., Christopher, P., Flytzani-Stephanopoulos, M., Stamatakis, M., Sykes, E.C.H., 2021. First-principles design of a single-atom-alloy propane dehydrogenation catalyst. Science 372, 1444–1447.

Hao, M., Qiu, M., Yang, H., Hu, B., Wang, X., 2021. Recent advances on preparation and environmental applications of MOF-derived carbons in catalysis. Sci. Total. Environ. 760, 143333.

He, C., Xiong, Y., Zhu, X., Li, X., 2004. A platinised TiO_2 film with both photocatalytic and non-photocatalytic activities towards the oxidation of formic acid. Appl. Catal. A-Gen. 275, 55–60.

He, C., Cheng, J., Zhang, X., Douthwaite, M., Pattisson, S., Hao, Z., 2019. Recent advances in the catalytic oxidation of volatile organic compounds: a review based on pollutant sorts and sources. Chem. Rev. 119, 4471–4568.

Hou, C.-C., Wang, H.-F., Li, C., Xu, Q., 2020. From metal–organic frameworks to single/dual-atom and cluster metal catalysts for energy applications. Energy Environ. Sci. 13, 1658–1693.

Huang, Y.S., Hsieh, C.C., 2019. Ambient volatile organic compound presence in the highly urbanized city: source apportionment and emission position. Atmos. Environ. 206, 45–59.

Hunt, S.T., Milina, M., Alba-Rubio, A.C., Hendon, C.H., Dumesic, J.A., Román-Leshkov, Y., 2016. Self-assembly of noble metal monolayers on transition metal carbide nanoparticle catalysts. Science 352, 974–978.

Ibrahim, R.K., Hayyan, M., AlSaadi, M.A., Hayyan, A., Ibrahim, S., 2016. Environmental application of nanotechnology: air, soil, and water. Environ. Sci. Pollut. Res. 23, 13754–13788.

Jiang, K., Siahrostami, S., Zheng, T., Hu, Y., Hwang, S., Stavitski, E., Peng, Y., Dynes, J., Gangisetty, M., Su, D., Attenkofer, K., Wang, H., 2018. Isolated Ni single atoms in graphene nanosheets for high-performance CO_2 reduction. Energy Environ. Sci. 11, 893–903.

Jiang, Q., Ao, Z., Li, S., Wen, Z., 2014. Density functional theory calculations on the CO catalytic oxidation on Al-embedded graphene. RSC Adv. 4, 20290–20296.

Jiang, Q., Zhang, J., Ao, Z., Huang, H., He, H., Wu, Y., 2018. First principles study on the CO oxidation on Mn-embedded divacancy graphene. Front. Chem. 6, 187.

Jiang, Q., Zhang, J., Huang, H., Wu, Y., Ao, Z., 2020. A novel single-atom catalyst for CO oxidation in humid environmental conditions: Ni-embedded divacancy graphene. J. Mater. Chem. A 8, 287–295.

Jones, C.W., 2018. Another nobel prize for catalysis: Frances arnold in 2018. ACS Catal. 8, 10913, 10913.

Kamal, M.S., Razzak, S.A., Hossain, M.M., 2016. Catalytic oxidation of volatile organic compounds (VOCs) – a review. Atmos. Environ. 140, 117–134.

Kaur, A., Kaur, G., Singh, P.P., Kaushal, S., 2021. Supported bimetallic nanoparticles as anode catalysts for direct methanol fuel cells: a review. Int. J. Hydrog. Energy 46, 15820–15849.

Kibria, M.G., Edwards, J.P., Gabardo, C.M., Dinh, C.-T., Seifitokaldani, A., Sinton, D., Sargent, E.H., 2019. Electrochemical CO_2 reduction into chemical feedstocks: from mechanistic electrocatalysis models to system design. Adv. Mater. 31, 1807166.

Kikkawa, S., Teramura, K., Asakura, H., Hosokawa, S., Tanaka, T., 2020. Ni–Pt alloy nanoparticles with isolated Pt atoms and their cooperative neighboring Ni atoms for selective hydrogenation of CO_2 toward CH_4 evolution: in situ and transient fourier transform infrared studies. ACS Appl. Nano Mater. 3, 9633–9644.

Kim, J., Roh, C.-W., Sahoo, S.K., Yang, S., Bae, J., Han, J.W., Lee, H., 2018. Highly durable platinum single-atom alloy catalyst for electrochemical reactions. Adv. Eng. Mater. 8, 1701476.

Kyriakou, G., Boucher, M.B., Jewell, A.D., Lewis, E.A., Lawton, T.J., Baber, A.E., Tierney, H.L., Flytzani-Stephanopoulos, M., Sykes, E.C.H., 2012. Isolated metal atom geometries as a strategy for selective heterogeneous hydrogenations. Science 335, 1209–1212.

Li, M., Duanmu, K., Wan, C., Cheng, T., Zhang, L., Dai, S., Chen, W., Zhao, Z., Li, P., Fei, H., Zhu, Y., Yu, R., Luo, J., Zang, K., Lin, Z., Ding, M., Huang, J., Sun, H., Guo, J., Pan, X., Goddard, W.A., Sautet, P., Huang, Y., Duan, X., 2019. Single-atom tailoring of platinum nanocatalysts for high-performance multifunctional electrocatalysis. Nat. Catal. 2, 495–503.

Li, M., Hua, B., Wang, L.-C., Zhou, Z., Stowers, K.J., Ding, D., 2020. Discovery of single-atom alloy catalysts for CO_2-to-methanol reaction by density functional theory calculations. Catal. Today.

Li, X., Yang, X., Huang, Y., Zhang, T., Liu, B., 2019. Supported noble-metal single atoms for heterogeneous catalysis. Adv. Mater. 31, 1902031.

Li, Z., He, T., Matsumura, D., Miao, S., Wu, A., Liu, L., Wu, G., Chen, P., 2017. Atomically dispersed Pt on the surface of Ni particles: synthesis and catalytic function in hydrogen generation from aqueous ammonia–borane. ACS Catal. 7, 6762–6769.

Li, Z., Ji, S., Liu, Y., Cao, X., Tian, S., Chen, Y., Niu, Z., Li, Y., 2020. Well-defined materials for heterogeneous catalysis: from nanoparticles to isolated single-atom sites. Chem. Rev. 120, 623–682.

Liu, B., Zhao, W., Jiang, Q., Ao, Z., An, T., 2019. Enhanced adsorption mechanism of carbonyl-containing volatile organic compounds on Al-decorated porous graphene monolayer: a density functional theory calculation study. Sustain. Mater. Technol. 21, e00103.

Liu, G., Zhou, J., Zhao, W., Ao, Z., An, T., 2020. Single atom catalytic oxidation mechanism of formaldehyde on Al doped graphene at room temperature. Chin. Chem. Lett. 31, 1966–1969.

Liu, J., Shan, J., Lucci, F.R., Cao, S., Sykes, E.C.H., Flytzani-Stephanopoulos, M., 2017. Palladium–gold single atom alloy catalysts for liquid phase selective hydrogenation of 1-hexyne. Catal. Sci. Technol. 7, 4276–4284.

Liu, J., Uhlman, M.B., Montemore, M.M., Trimpalis, A., Giannakakis, G., Shan, J., Cao, S., Hannagan, R.T., Sykes, E.C.H., Flytzani-Stephanopoulos, M., 2019. Integrated catalysis-surface science-theory approach to understand selectivity in the hydrogenation of 1-hexyne to 1-hexene on PdAu single-atom alloy catalysts. ACS Catal. 9, 8757–8765.

Liu, L., Corma, A., 2018. Metal catalysts for heterogeneous catalysis: From single atoms to nanoclusters and nanoparticles. Chem. Rev. 118, 4981–5079.

Liu, X., Ao, C., Shen, X., Wang, L., Wang, S., Cao, L., Zhang, W., Dong, J., Bao, J., Ding, T., Zhang, L., Yao, T., 2020. Dynamic surface reconstruction of single-atom bimetallic alloy under operando electrochemical conditions. Nano Lett. 20, 8319–8325.

Long, R., Li, Y., Liu, Y., Chen, S., Zheng, X., Gao, C., He, C., Chen, N., Qi, Z., Song, L., Jiang, J., Zhu, J., Xiong, Y., 2017. Isolation of Cu atoms in Pd lattice: forming highly selective sites for photocatalytic conversion of CO_2 to CH_4. J. Am. Chem. Soc. 139, 4486–4492.

Lopez-Acevedo, O., Kacprzak, K.A., Akola, J., Häkkinen, H., 2010. Quantum size effects in ambient CO oxidation catalysed by ligand-protected gold clusters. Nat. Chem. 2, 329–334.

Lu, J., Low, K.-B., Lei, Y., Libera, J.A., Nicholls, A., Stair, P.C., Elam, J.W., 2014. Toward atomically-precise synthesis of supported bimetallic nanoparticles using atomic layer deposition. Nat. Commun. 5, 3264.

Lu, Y., Zhang, Z., Lin, F., Wang, H., Wang, Y., 2020. Single-atom automobile exhaust catalysts. ChemNanoMat 6, 1659–1682.

Lucci, F.R., Lawton, T.J., Pronschinske, A., Sykes, E.C.H., 2014. Atomic scale surface structure of Pt/Cu(111) surface alloys. J. Phys. Chem. C 118, 3015–3022.

Lucci, F.R., Liu, J., Marcinkowski, M.D., Yang, M., Allard, L.F., Flytzani-Stephanopoulos, M., Sykes, E.C.H., 2015a. Selective hydrogenation of 1,3-butadiene on platinum–copper alloys at the single-atom limit. Nat. Commun. 6, 8550.

Lucci, F.R., Marcinkowski, M.D., Lawton, T.J., Sykes, E.C.H., 2015b. H_2 activation and spillover on catalytically relevant Pt–Cu single atom alloys. J. Phy. Chem. C 119, 24351–24357.

Lucci, F.R., Darby, M.T., Mattera, M.F.G., Ivimey, C.J., Therrien, A.J., Michaelides, A., Stamatakis, M., Sykes, E.C.H., 2016. Controlling hydrogen activation, spillover, and desorption with Pd–Au single-atom alloys. J. Phys. Chem. Lett. 7, 480–485.

Luneau, M., Shirman, T., Filie, A., Timoshenko, J., Chen, W., Trimpalis, A., Flytzani-Stephanopoulos, M., Kaxiras, E., Frenkel, A.I., Aizenberg, J., Friend, C.M., Madix, R. J., 2019. Dilute Pd/Au alloy nanoparticles embedded in colloid-templated porous SiO_2: stable Au-based oxidation catalysts. Chem. Mater. 31, 5759–5768.

Luo, S., Zhang, L., Liao, Y., Li, L., Yang, Q., Wu, X., Wu, X., He, D., He, C., Chen, W., Wu, Q., Li, M., Hensen, E.J.M., Quan, Z., 2021. A tensile-strained Pt–Rh single-atom alloy remarkably boosts ethanol oxidation. Adv. Mater. 33, 2008508.

Mao, J., Yin, J., Pei, J., Wang, D., Li, Y., 2020. Single atom alloy: An emerging atomic site material for catalytic applications. Nano Today 34, 100917.

Marcinkowski, M.D., Jewell, A.D., Stamatakis, M., Boucher, M.B., Lewis, E.A., Murphy, C.J., Kyriakou, G., Sykes, E.C.H., 2013. Controlling a spillover pathway with the molecular cork effect. Nat. Mater. 12, 523–528.

Marcinkowski, M.D., Darby, M.T., Liu, J., Wimble, J.M., Lucci, F.R., Lee, S., Michaelides, A., Flytzani-Stephanopoulos, M., Stamatakis, M., Sykes, E.C.H., 2018. Pt/Cu single-atom alloys as coke-resistant catalysts for efficient C–H activation. Nat. Chem. 10, 325–332.

Mashayekhi, N.A., Kung, M.C., Kung, H.H., 2014. Selective oxidation of hydrocarbons on supported Au catalysts. Catal. Today 238, 74–79.

Miura, H., Endo, K., Ogawa, R., Shishido, T., 2017. Supported palladium–gold alloy catalysts for efficient and selective hydrosilylation under mild conditions with isolated single palladium atoms in alloy nanoparticles as the main active site. ACS Catal. 7, 1543–1553.

Mohan, O., Xu, R., Mushrif, S.H., 2021. Novel nickel-based single-atom alloy catalyst for CO_2 conversion reactions: Computational screening and reaction mechanism analysis. J. Phys. Chem. C 125, 4041–4055.

Nørskov, J.K., Bligaard, T., Hvolbæk, B., Abild-Pedersen, F., Chorkendorff, I., Christensen, C.H., 2008. The nature of the active site in heterogeneous metal catalysis. Chem. Soc. Rev. 37, 2163–2171.

Nakaya, Y., Hirayama, J., Yamazoe, S., Shimizu, K.-i, Furukawa, S., 2020. Single-atom Pt in intermetallics as an ultrastable and selective catalyst for propane dehydrogenation. Nat. Commun. 11, 2838.

Neurock, M., Janik, M., Wieckowski, A., 2009. A first principles comparison of the mechanism and site requirements for the electrocatalytic oxidation of methanol and formic acid over Pt. Faraday Discuss. 140, 363–378.

Nigam, S., Majumder, C., 2018. Single atom alloy catalyst for SO_3 decomposition: Enhancement of platinum catalyst's performance by Ag atom embedding. Nanoscale 10, 20599–20610.

Nur, A.S.M., Matsukawa, T., Funada, E., Hinokuma, S., Machida, M., 2018. Platinum supported on Ta_2O_5 as a stable SO_3 decomposition catalyst for solar thermochemical water splitting cycles. ACS Appl. Energy Mater. 1, 744–750.

Ouyang, M., Papanikolaou, K.G., Boubnov, A., Hoffman, A.S., Giannakakis, G., Bare, S.R., Stamatakis, M., Flytzani-Stephanopoulos, M., Sykes, E.C.H., 2021. Directing reaction pathways via in situ control of active site geometries in PdAu single-atom alloy catalysts. Nat. Commun. 12, 1549.

Pan, Y., Yunyang, Q., Zheng, X., Chu, S.-Q., Yang, Y., Ding, C., Wang, X., Yu, S.-H., Jiang, H.-L., 2020. Precise fabrication of single-atom alloy co-catalyst with optimal charge state for enhanced photocatalysis. Natl. Sci. Rev. 24.

Papanikolaou, K.G., Stamatakis, M., 2021. The catalytic decomposition of nitrous oxide and the NO + CO reaction over Ni/Cu dilute and single atom alloy surfaces: first-principles microkinetic modelling. Catal. Sci. Technol. 11, 3681–3696.

Parvulescu, V.I., Fechete, I., 2018. Approach in green catalysis. Catal. Today 306, 1.

Patel, D.A., Hannagan, R.T., Kress, P.L., Schilling, A.C., Çınar, V., Sykes, E.C.H., 2019. Atomic-scale surface structure and CO tolerance of NiCu single-atom alloys. J. Phys. Chem. C 123, 28142–28147.

Pei, G.X., Liu, X.Y., Wang, A., Li, L., Huang, Y., Zhang, T., Lee, J.W., Jang, B.W.L., Mou, C.-Y., 2014. Promotional effect of Pd single atoms on Au nanoparticles supported on silica for the selective hydrogenation of acetylene in excess ethylene. New J. Chem. 38, 2043–2051.

Pei, G.X., Liu, X.Y., Wang, A., Lee, A.F., Isaacs, M.A., Li, L., Pan, X., Yang, X., Wang, X., Tai, Z., Wilson, K., Zhang, T., 2015. Ag alloyed Pd single-atom catalysts for efficient selective hydrogenation of acetylene to ethylene in excess ethylene. ACS Catal. 5, 3717–3725.

Pei, G.X., Liu, X.Y., Yang, X., Zhang, L., Wang, A., Li, L., Wang, H., Wang, X., Zhang, T., 2017. Performance of Cu-alloyed Pd single-atom catalyst for semihydrogenation of acetylene under simulated front-end conditions. ACS Catal. 7, 1491–1500.

Perreault, F., Fonseca de Faria, A., Elimelech, M., 2015. Environmental applications of graphene-based nanomaterials. Chem. Soc. Rev. 44, 5861–5896.

Prins, G., 2011. Climate change: beyond kyoto. Nature 474, 576–577.

Rajabi, H., Hadi Mosleh, M., Mandal, P., Lea-Langton, A., Sedighi, M., 2020. Emissions of volatile organic compounds from crude oil processing – global emission inventory and environmental release. Sci. Total. Environ. 727, 138654.

Randazzo, A., Asensio-Ramos, M., Melián, G.V., Venturi, S., Padrón, E., Hernández, P.A., Pérez, N.M., Tassi, F., 2020. Volatile organic compounds (VOCs) in solid waste landfill cover soil: chemical and isotopic composition vs. degradation processes. Sci. Total. Environ. 726, 138326.

Rezaei, M., 2021. Catalysis engineering for environmental applications. Process Saf. Environ. 149, 507.

Roy, S.C., Varghese, O.K., Paulose, M., Grimes, C.A., 2010. Toward solar fuels: photocatalytic conversion of carbon dioxide to hydrocarbons. ACS Nano 4, 1259–1278.

Salthammer, T., Zhang, Y., Mo, J., Koch, H.M., Weschler, C.J., 2018. Assessing human exposure to organic pollutants in the indoor environment. Angew. Chem. Int. Ed. 57, 12228–12263.

Shan, J., Lucci, F.R., Liu, J., El-Soda, M., Marcinkowski, M.D., Allard, L.F., Sykes, E.C.H., Flytzani-Stephanopoulos, M., 2016. Water co-catalyzed selective dehydrogenation of methanol to formaldehyde and hydrogen. Surf. Sci. 650, 121–129.

Shan, J., Janvelyan, N., Li, H., Liu, J., Egle, T.M., Ye, J., Biener, M.M., Biener, J., Friend, C.M., Flytzani-Stephanopoulos, M., 2017. Selective non-oxidative dehydrogenation of ethanol to acetaldehyde and hydrogen on highly dilute NiCu alloys. Appl. Catal. B-Environ. 205, 541–550.

Shan, J., Liu, J., Li, M., Lustig, S., Lee, S., Flytzani-Stephanopoulos, M., 2018. NiCu single atom alloys catalyze the C-H bond activation in the selective non-oxidative ethanol dehydrogenation reaction. Appl. Catal. B-Environ. 226, 534–543.

Sharif, H.M.A., Mahmood, N., Wang, S., Hussain, I., Hou, Y.-N., Yang, L.-H., Zhao, X., Yang, B., 2021. Recent advances in hybrid wet scrubbing techniques for NO_x and SO_2 removal: State of the art and future research. Chemosphere 273, 129695.

Shen, T., Zhang, J., Chen, K., Deng, S., Wang, D., 2020. Recent progress of palladium-based electrocatalysts for the formic acid oxidation reaction. Energy Fuels 34, 9137–9153.

Sheng, W., Kattel, S., Yao, S., Yan, B., Liang, Z., Hawxhurst, C.J., Wu, Q., Chen, J.G., 2017. Electrochemical reduction of CO_2 to synthesis gas with controlled CO/H_2 ratios. Energy Environ. Sci. 10, 1180–1185.

Shimizu, K.-i, Satsuma, A., 2011. Toward a rational control of solid acid catalysis for green synthesis and biomass conversion. Energy Environ. Sci. 4, 3140–3153.

Silas, K., Wan Ab Karim Ghani, W.A., Choong, T.S.Y., Rashid, U., 2020. Monolith metal-oxide-supported catalysts: sorbent for environmental application. Catalysts 10, 1018.

Siwal, S.S., Thakur, S., Zhang, Q.B., Thakur, V.K., 2019. Electrocatalysts for electrooxidation of direct alcohol fuel cell: chemistry and applications. Mater. Today Chem. 14, 100182.

Song, C., Liu, Y., Sun, L., Zhang, Q., Mao, H., 2020. Emissions of volatile organic compounds (VOCs) from gasoline- and liquified natural gas (LNG)-fueled vehicles in tunnel studies. Atmos. Environ. 234, 117626.

Sordakis, K., Tang, C., Vogt, L.K., Junge, H., Dyson, P.J., Beller, M., Laurenczy, G., 2018. Homogeneous catalysis for sustainable hydrogen storage in formic acid and alcohols. Chem. Rev. 118, 372–433.

Stevanović, S., Tripković, D., Tripković, V., Minić, D., Gavrilović, A., Tripković, A., Jovanović, V.M., 2014. Insight into the effect of Sn on CO and formic acid oxidation at PtSn catalysts. J. Phys. Chem. C 118, 278–289.

Sui, L., An, W., Feng, Y., Wang, Z., Zhou, J., Hur, S.H., 2020. Bimetallic Pd-based surface alloys promote electrochemical oxidation of formic acid: mechanism, kinetics and descriptor. J. Power Sources 451, 227830.

Sun, G., Zhao, Z.-J., Mu, R., Zha, S., Li, L., Chen, S., Zang, K., Luo, J., Li, Z., Purdy, S.C., Kropf, A.J., Miller, J.T., Zeng, L., Gong, J., 2018. Breaking the scaling relationship via thermally stable Pt/Cu single atom alloys for catalytic dehydrogenation. Nat. Commun. 9, 4454.

Sun, L., Reddu, V., Fisher, A.C., Wang, X., 2020. Electrocatalytic reduction of carbon dioxide: opportunities with heterogeneous molecular catalysts. Energy Environ. Sci. 13, 374–403.

Sun, S., Sun, G., Pei, C., Zhao, Z.-J., Gong, J., 2021. Origin of performances of Pt/Cu single-atom alloy catalysts for propane dehydrogenation. J. Phys. Chem. C 125, 18708–18716.

Tackett, B.M., Gomez, E., Chen, J.G., 2019. Net reduction of CO_2 via its thermocatalytic and electrocatalytic transformation reactions in standard and hybrid processes. Nat. Catal. 2, 381–386.

Tackett, B.M., Lee, J.H., Chen, J.G., 2020. Electrochemical conversion of CO_2 to syngas with palladium-based electrocatalysts. Acc. Chem. Res. 53, 1535–1544.

Tao, H., Sun, X., Back, S., Han, Z., Zhu, Q., Robertson, Alex, W., Ma, T., Fan, Q., Han, B., Jung, Y., Sun, Z., 2018. Doping palladium with tellurium for the highly selective electrocatalytic reduction of aqueous CO_2 to CO. Chem. Sci. 9, 483–487.

Tsai, W.-T., 2018. An overview of health hazards of volatile organic compounds regulated as indoor air pollutants. Rev. Environ. Health 34.

van Santen, R.A., Neurock, M., Shetty, S.G., 2010. Reactivity theory of transition-metal surfaces: a brønsted−evans−polanyi linear activation energy−free-energy analysis. Chem. Rev 2005–2048.

Wang, A., Li, J., Zhang, T., 2018. Heterogeneous single-atom catalysis. Nat. Rev. Chem. 2, 65–81.

Wang, C., Garbarino, G., Allard, L.F., Wilson, F., Busca, G., Flytzani-Stephanopoulos, M., 2016. Low-temperature dehydrogenation of ethanol on atomically dispersed gold supported on $ZnZrO_x$. ACS Catal. 6, 210–218.

Wang, H., Jiao, L., Zheng, L., Fang, Q., Qin, Y., Luo, X., Wei, X., Hu, L., Gu, W., Wen, J., Zhu, C., 2021. PdBi single-atom alloy aerogels for efficient ethanol oxidation. Adv. Funct. Mater. 31, 2103465.

Wang, H., Luo, Q., Liu, W., Lin, Y., Guan, Q., Zheng, X., Pan, H., Zhu, J., Sun, Z., Wei, S., Yang, J., Lu, J., 2019. Quasi Pd_1Ni single-atom surface alloy catalyst enables hydrogenation of nitriles to secondary amines. Nat. Commun. 10, 4998.

Wang, T., Nie, C., Ao, Z., Wang, S., An, T., 2020. Recent progress in g-C_3N_4 quantum dots: synthesis, properties and applications in photocatalytic degradation of organic pollutants. J. Mater. Chem. A 8, 485–502.

Wang, Z.-T., Hoyt, R.A., El-Soda, M., Madix, R.J., Kaxiras, E., Sykes, E.C.H., 2018. Dry dehydrogenation of ethanol on Pt–Cu single atom alloys. Top. Catal. 61, 328–335.

Wen, C., Yin, A., Dai, W.-L., 2014. Recent advances in silver-based heterogeneous catalysts for green chemistry processes. Appl. Catal. B-Environ. 160–161, 730–741.

Wen, H., Huai, L.-y, Jin, X., Liu, J.-y, 2019. Mechanism of nitric oxide reduction by hydrogen on Ni(110) and Ir/Ni(110): First principles and microkinetic modeling. J. Phys. Chem. C 123, 4825–4836.

Weon, S., Huang, D., Rigby, K., Chu, C., Wu, X., Kim, J.-H., 2021. Environmental materials beyond and below the nanoscale: Single-atom catalysts. ACS EST Eng. 1, 157–172.

Wrasman, C.J., Boubnov, A., Riscoe, A.R., Hoffman, A.S., Bare, S.R., Cargnello, M., 2018. Synthesis of colloidal Pd/Au dilute alloy nanocrystals and their potential for selective catalytic oxidations. J. Am. Chem. Soc. 140, 12930–12939.

Wrasman, C.J., Riscoe, A.R., Lee, H., Cargnello, M., 2020. Dilute Pd/Au alloys replace Au/TiO_2 interface for selective oxidation reactions. ACS Catal. 10, 1716–1720.

Xi, Z., Lv, H., Erdosy, D.P., Su, D., Li, Q., Yu, C., Li, J., Sun, S., 2017. Atomic scale deposition of Pt around Au nanoparticles to achieve much enhanced electrocatalysis of Pt. Nanoscale 9, 7745–7749.

Xia, X., Wang, Y., Ruditskiy, A., Xia, Y., 2013. 25th anniversary article: galvanic replacement: a simple and versatile route to hollow nanostructures with tunable and well-controlled properties. Adv. Mater. 25, 6313–6333.

Xie, H., Wan, Y., Wang, X., Liang, J., Lu, G., Wang, T., Chai, G., Adli, N.M., Priest, C., Huang, Y., Wu, G., Li, Q., 2021. Boosting Pd-catalysis for electrochemical CO_2 reduction to CO on Bi-Pd single atom alloy nanodendrites. Appl. Catal. B-Environ. 289, 119783.

Xing, F., Jeon, J., Toyao, T., Shimizu, K.-i, Furukawa, S., 2019. A Cu–Pd single-atom alloy catalyst for highly efficient NO reduction. Chem. Sci. 10, 8292–8298.

Yang, C., Miao, Z., Zhang, F., Li, L., Liu, Y., Wang, A., Zhang, T., 2018. Hydrogenolysis of methyl glycolate to ethanol over a Pt–Cu/SiO_2 single-atom alloy catalyst: a further step from cellulose to ethanol. Green Chem. 20, 2142–2150.

Yang, J., Li, W., Wang, D., Li, Y., 2021. Single-atom materials: small structures determine macroproperties. Small Struct. 2, 2000051.

Yang, K., Yang, B., 2018. Identification of the active and selective sites over a single Pt atom-alloyed Cu catalyst for the hydrogenation of 1,3-butadiene: a combined DFT and microkinetic modeling study. J. Phys. Chem. C 122, 10883–10891.

Yang, X.-F., Wang, A., Qiao, B., Li, J., Liu, J., Zhang, T., 2013. Single-atom catalysts: a new frontier in heterogeneous catalysis. Acc. Chem. Res. 46, 1740–1748.

Yuan, L., Hung, S.-F., Tang, Z.-R., Chen, H.M., Xiong, Y., Xu, Y.-J., 2019. Dynamic evolution of atomically dispersed Cu species for CO_2 photoreduction to solar fuels. ACS Catal. 9, 4824–4833.

Zhang, H., Kawashima, K., Okumura, M., Toshima, N., 2014. Colloidal Au single-atom catalysts embedded on Pd nanoclusters. J. Mater. Chem. A 2, 13498–13508.

Zhang, L., Wang, A., Miller, J.T., Liu, X., Yang, X., Wang, W., Li, L., Huang, Y., Mou, C.-Y., Zhang, T., 2014. Efficient and durable Au alloyed Pd single-atom catalyst for the ullmann reaction of aryl chlorides in water. ACS Catal. 4, 1546–1553.

Zhang, L., Liu, H., Liu, S., Norouzi Banis, M., Song, Z., Li, J., Yang, L., Markiewicz, M., Zhao, Y., Li, R., Zheng, M., Ye, S., Zhao, Z.-J., Botton, G.A., Sun, X., 2019. Pt/Pd single-atom alloys as highly active electrochemical catalysts and the origin of enhanced activity. ACS Catal. 9, 9350–9358.

Zhang, N., Ye, C., Yan, H., Li, L., He, H., Wang, D., Li, Y., 2020. Single-atom site catalysts for environmental catalysis. Nano Res. 13, 3165–3182.

Zhang, S., Nguyen, L., Liang, J.-X., Shan, J., Liu, J., Frenkel, A.I., Patlolla, A., Huang, W., Li, J., Tao, F., 2015. Catalysis on singly dispersed bimetallic sites. Nat. Commun. 6, 7938.

Zhang, S., Rong, H., Yang, T., Bai, B., Zhang, J., 2020. Ultrafine PtRu dilute alloy nanodendrites for enhanced electrocatalytic methanol oxidation. Chem. Eur. J. 26, 4025–4031.

Zhang, T., Walsh, A.G., Yu, J., Zhang, P., 2021. Single-atom alloy catalysts: structural analysis, electronic properties and catalytic activities. Chem. Soc. Rev. 50, 569–588.

Zhang, X., Cui, G., Feng, H., Chen, L., Wang, H., Wang, B., Zhang, X., Zheng, L., Hong, S., Wei, M., 2019. Platinum–copper single atom alloy catalysts with high performance towards glycerol hydrogenolysis. Nat. Commun. 10, 5812.

Zhang, Y.-J., Sethuraman, V., Michalsky, R., Peterson, A.A., 2014. Competition between CO_2 reduction and H_2 evolution on transition-metal electrocatalysts. ACS Catal. 4, 3742–3748.

Zhang, Y.-n., Niu, Q., Gu, X., Yang, N., Zhao, G., 2019. Recent progress on carbon nanomaterials for the electrochemical detection and removal of environmental pollutants. Nanoscale 11, 11992–12014.

Zhang, Y., Shi, X.-R., Sun, C., Huang, S., Duan, Z., Ma, P., Wang, J., 2020. CO oxidation on Ni-based single-atom alloys surfaces. Mol. Catal. 495, 111154.

Zhang, Y., Wang, B., Fan, M., Li, D., Zhang, R., 2021. Ethane dehydrogenation over the single-atom alloy catalysts: screening out the excellent catalyst with the dual descriptors. Fuel 306, 121641.

Zhao, Y., Liu, X., Chen, D., Liu, Z., Yang, Q., Lin, X., Peng, M., Liu, P., Tan, Y., 2021. Atomic-level-designed copper atoms on hierarchically porous gold architectures for high-efficiency electrochemical CO_2 reduction. Sci. China Mater. 64, 1900–1909.

Zhi, X., Jiao, Y., Zheng, Y., Vasileff, A., Qiao, S.-Z., 2020. Selectivity roadmap for electrochemical CO_2 reduction on copper-based alloy catalysts. Nano Energy 71, 104601.

Zhou, J., Ao, Z., An, T., 2021. DFT study of the decomposition mechanism of H_2S on v-decorated Ti_2CO_2 single-atom catalyst. Acta Phys. -Chim. Sin. 37, 2007086.